

## Structural variety of isopropyl-bis(2-picoly)amine complexes with zinc(II) and copper(II)

Natalija Pantalon Juraj, Senada Muratovi#, Berislav Peric, Natasa Sijakovic Vujicic, Robert Vianello, Dijana Žili#, Zvonko Jaglicic, and Sre#ko I. Kirin

*Cryst. Growth Des.*, **Just Accepted Manuscript** • DOI: 10.1021/acs.cgd.9b01625 • Publication Date (Web): 20 Feb 2020

Downloaded from [pubs.acs.org](https://pubs.acs.org) on February 23, 2020

### Just Accepted

“Just Accepted” manuscripts have been peer-reviewed and accepted for publication. They are posted online prior to technical editing, formatting for publication and author proofing. The American Chemical Society provides “Just Accepted” as a service to the research community to expedite the dissemination of scientific material as soon as possible after acceptance. “Just Accepted” manuscripts appear in full in PDF format accompanied by an HTML abstract. “Just Accepted” manuscripts have been fully peer reviewed, but should not be considered the official version of record. They are citable by the Digital Object Identifier (DOI®). “Just Accepted” is an optional service offered to authors. Therefore, the “Just Accepted” Web site may not include all articles that will be published in the journal. After a manuscript is technically edited and formatted, it will be removed from the “Just Accepted” Web site and published as an ASAP article. Note that technical editing may introduce minor changes to the manuscript text and/or graphics which could affect content, and all legal disclaimers and ethical guidelines that apply to the journal pertain. ACS cannot be held responsible for errors or consequences arising from the use of information contained in these “Just Accepted” manuscripts.

# Structural Variety of Isopropyl-bis(2-picolyl)amine Complexes with Zinc(II) and Copper(II)

Natalija Pantalon Juraj,<sup>a</sup> Senada Muratović,<sup>a</sup> Berislav Perić,<sup>a</sup> Nataša Šijaković Vujičić,<sup>a</sup> Robert Vianello,<sup>a</sup> Dijana Žilić,<sup>a</sup> Zvonko Jagličić<sup>b</sup> and Srećko I. Kirin<sup>a,\*</sup>

<sup>a</sup>Ruđer Bošković Institute, Bijenička c. 54, HR-10000 Zagreb, Croatia

<sup>b</sup>Institute of Mathematics, Physics and Mechanics & Faculty of Civil and Geodetic Engineering University of Ljubljana, Jamova 2, 1000 Ljubljana, Slovenia

**ABSTRACT:** A variety of structurally different complexes of the isopropyl-bis(2-picolyl)amine (**iPr-bpa**) ligand were prepared with  $ZnA_2$  and  $CuA_2$  salts ( $A = Br^-$ ,  $Br^-/PF_6^-$ ,  $BF_4^-/F^-$ ,  $ClO_4^-$ ). The choice of different counterion affected the stoichiometry, coordination number, geometry and formation of geometrical isomers. Crystal structures of four Zn(II) complexes; two monomers (*mer*-[Zn(**iPr-bpa**)Br<sub>2</sub>] and *fac*-[Zn(**iPr-bpa**)Br<sub>2</sub>]), one F<sup>-</sup> bridged dimer ([Zn<sub>2</sub>(μ-F)<sub>2</sub>(**iPr-bpa**)<sub>2</sub>](BF<sub>4</sub>)<sub>2</sub>) and one ML<sub>2</sub> complex ([Zn(**iPr-bpa**)<sub>2</sub>](ClO<sub>4</sub>)<sub>2</sub>) were determined, and their solution structures were studied by NMR spectroscopy. For the ML<sub>2</sub> complex, relative stabilities of geometrical isomers were determined using DFT calculations. For Cu(II) complexes, five crystal structures were determined; two monomers ([Cu(**iPr-bpa**)Br<sub>2</sub>] and [Cu(**iPr-bpa**)(ClO<sub>4</sub>)<sub>2</sub>(H<sub>2</sub>O)]), a Br<sup>-</sup> bridged dimer ([Cu<sub>2</sub>(μ-Br)(Br)<sub>2</sub>(**iPr-bpa**)<sub>2</sub>](PF<sub>6</sub>) × CH<sub>3</sub>OH), a F<sup>-</sup> bridged coordination polymer ([Cu(μ-F)(**iPr-bpa**)<sub>n</sub>](BF<sub>4</sub>)<sub>n</sub> × nCH<sub>3</sub>OH), and a cyclic, CO<sub>3</sub><sup>2-</sup> bridged trimer ([Cu<sub>3</sub>(tri-μ-CO<sub>3</sub>)(ClO<sub>4</sub>)<sub>3</sub>(**iPr-bpa**)<sub>3</sub>](ClO<sub>4</sub>)). The different crystallographic structures of Cu(II) complexes are reflected in their different magnetic properties investigated by ESR spectroscopy and magnetic susceptibility measurements.

## Introduction

Transition metal complexes of the bis(2-picolyl)amine (**bpa**) ligand are extensively studied in literature; the Zn(II) and Cu(II) **bpa** complexes find use as enzyme mimics for structural features or function,<sup>1-4</sup> promising anticancer agents,<sup>5,6</sup> potent metal ion sensors,<sup>7-9</sup> and selective catalysts.<sup>10,11</sup> A particular focus of recent research efforts are various effects that govern the formation of complexes of different stoichiometry, coordination numbers and coordination geometry, including geometrical isomers.<sup>12</sup> The contributing effects include the electronic or steric properties of the ligand,<sup>13</sup> and the coordinating ability of the counterion.<sup>14</sup>

Transition metal complexes of the **bpa** ligand with ML<sub>2</sub> stoichiometry are found as both *trans*- and *cis-fac* isomers, apparently influenced by the coordinating ability of the counterion and the substituent on the central amine nitrogen. All published ML<sub>2</sub> complexes of **R-bpa** ligands with R ≠ H are *cis-fac* isomers in the solid state,<sup>15,16</sup> while both *cis*- and *trans-fac* isomers are reported for **R-bpa** (R = H) ligands, the *cis-fac* predominantly forming when weakly coordinating anions were used in the synthesis.<sup>17,18</sup> In the Cambridge Structural Database CSD, there is also a significant number of bridged **bpa** metal complexes, mostly the bridging functional groups are hydroxide or halogenide ions.<sup>19,20</sup>

Recently, we have reported on metal complexes of **bpa** and iminodiacetamide (**imda**) ligands.<sup>21,22</sup> Both **bpa** and **imda** ligands are tridentate with a central amine nitrogen atom substituted with two methylene pyridine (**bpa**) or methylene

acetamide (**imda**) moieties. Interestingly, despite their similarity in structure, the two ligand systems differ significantly in their stereochemical preference for formation of ML<sub>2</sub> complexes. In particular, **imda** ligands form almost exclusively *trans-fac*, while **bpa** ligands gave preferentially ML<sub>2</sub> *cis-fac* isomers (Figure 1). Herein, we aim to prepare complexes of ML<sub>2</sub> stoichiometry and study the stability of their different geometrical isomers. We focused on the effect of the counterion, preparing complexes of ligand **iPr-bpa** (**L**) with Zn(II) or Cu(II) and different counterions (Br<sup>-</sup>, Br<sup>-</sup>/PF<sub>6</sub><sup>-</sup>, BF<sub>4</sub><sup>-</sup>/F<sup>-</sup>, ClO<sub>4</sub><sup>-</sup>). Of the four crystal structures of Zn(II) complexes, two of the structures were found to be polymorphs (**1azn** and **1bzn**) and the stability of the two pol-

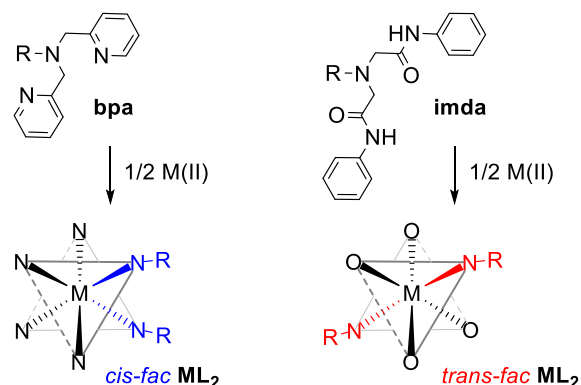


Figure 1. Different stereochemical preference of ML<sub>2</sub> complexes with **bpa** and **imda** ligands.

ymorphs was studied by differential scanning calorimetry and DFT calculations. The solution structure of the Zn(II) complexes was studied by nuclear magnetic resonance (NMR) spectroscopy. Five crystal structures of Cu(II) complexes were determined and their local magnetic properties studied by electron spin/paramagnetic resonance ESR/EPR spectroscopy and magnetic susceptibility measurements. Additionally, the CO<sub>2</sub> binding properties of **3b<sub>Cu</sub>** were studied by UV-Vis spectroscopy.

## Results and discussion

### Synthesis and characterization of Zn(II) complexes

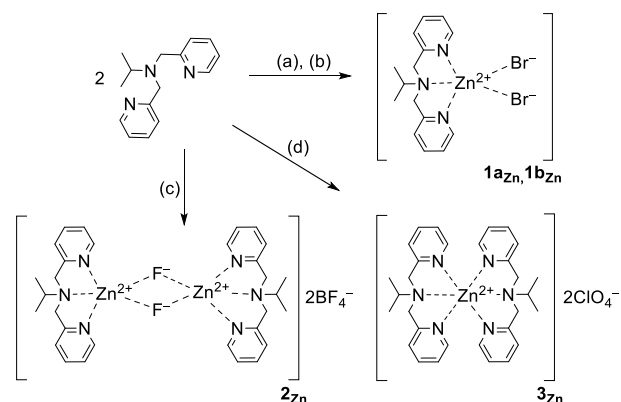
Four complexes were prepared using the ligand **iPr-bpa** and several different Zn(II) salts; two polymorphs, **1a<sub>Zn</sub>** and **1b<sub>Zn</sub>**, a bridged dimer **2<sub>Zn</sub>** and a ML<sub>2</sub> complex **3<sub>Zn</sub>** (Scheme 1). Their molecular structures determined by single crystal X-ray crystallography are shown in Figure 2 and selected bond lengths are collected in Table 1.

Attempting to prepare a complex of ML<sub>2</sub> stoichiometry, **iPr-bpa** and ZnBr<sub>2</sub> were mixed in a 2:1 ratio. However, due to the strong coordinating ability of the bromide anion, a complex of ML stoichiometry was obtained, namely **1a<sub>Zn</sub>**.<sup>21</sup> The solid state structure of **1a<sub>Zn</sub>** was determined using single crystal X-ray diffraction. Complex **1a<sub>Zn</sub>** contains two independent molecules in the unit cell. Both independent molecules of **1a<sub>Zn</sub>** are penta-coordinated, having distorted square pyramidal [ZnBr<sub>2</sub>N<sub>3</sub>] geometry ( $\tau_1 = 0.34$  and  $\tau_2 = 0.17$ , respectively)<sup>23</sup>, where the ligand is coordinated meridionally [angle N<sub>1</sub>–Zn–N<sub>3</sub> = 152.36(10)° for Zn<sub>1</sub> and 150.34(10)° for Zn<sub>2</sub>, angles between pyridine planes are 12.19(15)° and 10.88(15)°, respectively]. The remaining two coordination sites of the central zinc cation are occupied by bromide anions.

In the synthesis using **iPr-bpa**, ZnBr<sub>2</sub> and NH<sub>4</sub>PF<sub>6</sub> in a ratio of 1:1:2, complex **1b<sub>Zn</sub>** was obtained. In the crystal structure of **1b<sub>Zn</sub>**, the PF<sub>6</sub><sup>−</sup> anion was not incorporated, but it was a polymorph of **1a<sub>Zn</sub>**, with a penta-coordinated zinc atom and ML stoichiometry. As opposed to **1a<sub>Zn</sub>**, in **1b<sub>Zn</sub>** the ligand is coordinated facially [angle N<sub>1</sub>–Zn–N<sub>3</sub> = 109.56(15)°, angle between pyridine planes = 79.1(2)°]. The [ZnBr<sub>2</sub>N<sub>3</sub>] coordination polyhedron in **1b<sub>Zn</sub>** is at the border between a trigonal bipyramid and square pyramid ( $\tau = 0.50$ ).

A survey of the CSD revealed that in the few known penta-coordinated [Zn(R-bpa)Br<sub>2</sub>] complexes the **bpa** ligand is bound to the central metal as *mer*-isomer.<sup>5,6,21,24,25</sup> On the other hand, even for a significantly broader class of com-

### Scheme 1. Synthesis of Zn(II) complexes<sup>a</sup>



<sup>a</sup>Reaction conditions: (a) ZnBr<sub>2</sub>, methanol; (b) 2 ZnBr<sub>2</sub>, 4 NH<sub>4</sub>PF<sub>6</sub>, methanol, (c) Zn(BF<sub>4</sub>)<sub>2</sub>, methanol; (d) Zn(ClO<sub>4</sub>)<sub>2</sub>,

pounds, namely [M(R-bpa)X<sub>2</sub>] complexes containing any transition metal M or any halogen ions X, the *bpa fac*-isomer was found relatively rarely in the solid state, with only a handful of structures in the literature.<sup>12,26–30</sup>

To study the conditions for the formation of the two polymorphs, **1a<sub>Zn</sub>** (*mer*) and **1b<sub>Zn</sub>** (*fac*), syntheses in different conditions were performed (Table S8). The phase purity of the obtained polycrystalline samples was analyzed with X-ray powder diffraction. During numerous attempts of crystallization, formation of the *mer* polymorph was observed more frequently, while in crystallizations using diethyl-ether diffusion the more frequently obtained polymorph was *fac*.

The stability of the two polymorphs was studied by differential scanning calorimetry and hot-stage microscopy, revealing a solid-to-solid polymorph transition from the polymorph *fac* to the more stable polymorph *mer* (Figure 3 and Figures S19–S22). The DSC heating curves of the *mer* polymorph showed only one endothermic transition with peak maximum at 266,6 °C and enthalpy change of  $\Delta H = 6.1$  kcal mol<sup>−1</sup> (Figure 3). The DSC thermograms of the *fac* polymorph showed two endothermic transitions; the first transition with peak maximum at 186,7 °C and enthalpy change of  $\Delta H = 1.6$  kcal mol<sup>−1</sup> and the second one at 264,7 °C and enthalpy change of 6.2 kcal mol<sup>−1</sup>.

Having compared the DSC thermograms of polymorph *fac* subjected to different heating-cooling procedures, we con-

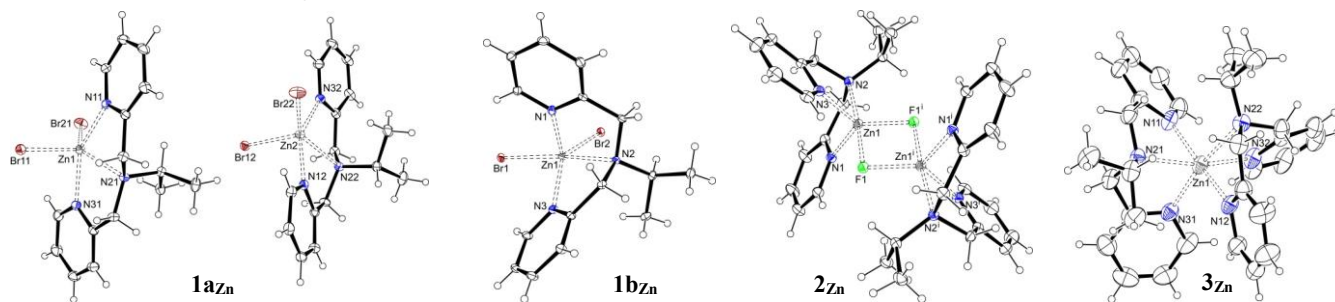


Figure 2. Molecular structures of complexes **1a<sub>Zn</sub>** (*mer*-[Zn(**iPr-bpa**)Br<sub>2</sub>]), **1b<sub>Zn</sub>** (*fac*-[Zn(**iPr-bpa**)Br<sub>2</sub>]), **2<sub>Zn</sub>** ([Zn<sub>2</sub>(μ-F)<sub>2</sub>(**iPr-bpa**)<sub>2</sub>](BF<sub>4</sub>)<sub>2</sub>) and **3<sub>Zn</sub>** ([Zn(**iPr-bpa**)<sub>2</sub>](ClO<sub>4</sub>)<sub>2</sub>). Displacement ellipsoids were drawn at the 30% probability level. The anions tetrafluoroborate (in **2<sub>Zn</sub>**) and perchlorate (in **3<sub>Zn</sub>**) were omitted for clarity.

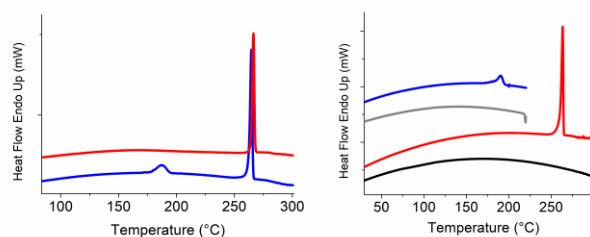


Figure 3. DSC thermograms of a) heating cycles of  $1a_{Zn}$  (*mer*, red) and  $1b_{Zn}$  (*fac*, blue); b) temperature-controlled transition of *fac* to *mer* polymorph.

cluded that the first endothermic transition corresponds to the *fac* to *mer* conversion process. This was confirmed by X-ray powder diffraction analysis of the sample of the *fac* polymorph heated to 220 °C and cooled to room temperature that showed the pattern of the *mer* polymorph (Figure S21). The enthalpy change of the second endothermic transition at 264 °C corresponds to melting of polymorph *mer*.

Computational analysis shows that *mer*  $1a_{Zn}$  is by 1.1 kcal mol<sup>-1</sup> on the Gibbs free-energy scale, and by 1.5 kcal mol<sup>-1</sup> on the enthalpy scale, more stable than its *fac*  $1b_{Zn}$  analogue, placing this result in firm agreement with experiments, thus confirming the higher thermodynamic stability and solution prevalence of the former. In addition, the transition state structure connecting these two isoforms lies only 7.4 kcal mol<sup>-1</sup> above the more stable  $1a_{Zn}$ , confirming that the transition between polymorphs is feasible even at room temperature.

The lattice energies of conformational polymorphs are very close and differences in  $\Delta H$  between 0.05 and 2.4 kcal mol<sup>-1</sup> have been reported for polymorphic transitions<sup>31–33</sup>. In this particular case there is a noticeable difference in energy and structure for the two polymorphs due to the different geometry of the complexes. In agreement with this conclusion, the hot-stage polarizing optical microscopy images in Figure S22 clearly showed the melting transition of crystals at 270 °C, and a small change during interconversion from the polymorph *fac* to polymorph *mer*.

In the next attempt of preparing a complex of  $ML_2$  stoichiometry, *iPr*-**bpa** and  $Zn(BF_4)_2$  were mixed in a 2:1 ratio. The tetrafluoroborate counterion was chosen as a weakly coordinating anion that would not interfere with binding of the second ligand to the metal. However, in these conditions the tetrafluoroborate ion undergoes a decomposition reaction,

$BF_4^- \rightleftharpoons BF_3 + F^-$ , forming fluoride ions. Fluorinated counterions like  $BF_4^-$  are known to be potential sources of fluoride ions.<sup>22,34,35</sup> The counterion decomposition could be accelerated by the basicity of the *iPr*-**bpa** ligand and/or by the metal, oxygen and water.<sup>20,36</sup> The free fluoride ion, being a small ion of localized charge, can easily bind to the metal center. The crystal structure of  $2_{Zn}$  shows a complex of  $M_2L_2$  stoichiometry, with two bridging fluoride anions. Complex  $2_{Zn}$  is centrosymmetric with penta-coordinated Zn(II) atoms,  $[ZnN_3(\mu-F)_2ZnN_3]$ , revealing two trigonal bipyramidal coordination polyhedrons ( $\tau_c = 0.86$ ) that share one edge. In  $2_{Zn}$ , the ligands are coordinated facially, with an  $N_1-Zn-N_3$  angle of  $111.44(7)^\circ$  and an angle between pyridine planes of  $79.30(12)^\circ$ . In the literature, only one zinc **bpa** complex is known with a double fluoride bridge,  $[(bpa)Zn(\mu-F)_2Zn(bpa)]$ ,<sup>37</sup> but several similar structures are published with other transition metals including iron, cobalt, nickel and copper.<sup>20,38–42</sup>

To avoid decomposition of the anion, perchlorate anion was used instead of tetrafluoroborate. The perchlorate anion is also weakly coordinating, but it is more stable in the applied reaction conditions. Complex  $3_{Zn}$  was prepared using *iPr*-**bpa** and  $Zn(ClO_4)_2$  in a 2:1 ratio, yielding a complex of  $ML_2$  stoichiometry as determined by single crystal X-ray diffraction. The two ligands in  $3_{Zn}$  are coordinated facially, with angles  $N_1-Zn-N_3$   $91.9(3)^\circ$  and  $93.5(3)^\circ$ , and the angle between pyridine planes =  $81.1(5)^\circ$  and  $82.3(6)^\circ$ , respectively. The hexa-coordinated complex  $3_{Zn}$  forms a  $[ZnN_6]$  distorted octahedron of *cis-fac* geometry [angle  $N-Zn-N$  (amine)  $102.9(2)^\circ$ ]. Our interest is to study effects that govern the formation of different geometrical isomers in  $ML_2$  complexes<sup>21,22</sup>, therefore we described the relative stability of *cis-fac*, *mer* and *trans-fac* isomers using DFT calculations. Our approach relied on optimizing molecular geometries with the  $Mo5-2X/6-31+G(d)/LanL2DZ + ECP$  model both in gas-phase and acetonitrile, the latter modeled through the implicit SMD solvation, being in line with our earlier reports.<sup>21,22</sup> The quality of this methodology was evaluated by performing a series of single-point electronic energy calculations using a range of DFT functionals. The respective relative energies are displayed in Table 2; selected bond lengths, angles and coordination geometries of the calculated geometrical isomers of  $[Zn(iPr-bpa)_2]^{2+}$  and  $[Zn(Me-bpa)_2]^{2+}$  are shown in Tables S6 and S7 and compared to the experimentally determined structures  $3_{Zn}$  and  $[Zn(bpa-CH_2-CH_2-CO_2Me)_2](BF_4)_2$  (from ref. 21). The results reveal a very good performance of the  $Mo5-2X$  functional, which gives trends in a close agreement with a majority of tested approaches, particularly with dispersion-corrected functionals such as  $\omega$ -B97XD, B97D3 and

Table 1. Selected bond lengths (Å) for Zn(II) complexes.

Complex	Zn–N <sub>1</sub> (Å)	Zn–N <sub>2</sub> (Å)	Zn–N <sub>3</sub> (Å)	Zn–anion (Å)
$1a_{Zn}$	2.177(2)	2.215(2)	2.162(2)	2.4061(5) (Br11); 2.4075(5) (Br21)
	2.142(2)	2.270(2)	2.143(2)	2.4188(5) (Br12); 2.4165(4) (Br22)
$1b_{Zn}$	2.073(4)	2.338(4)	2.101(4)	2.5079(7) (Br1); 2.4247(7) (Br2)
$2_{Zn}$	2.0371(17)	2.1717(16)	2.0269(17)	2.0462(12) (F1); 1.9313(11) (F1')
$3_{Zn}$	2.229(9)	2.287(7)	2.100(7)	—
	2.195(9)	2.417(7)	2.155(8)	—

**Table 2. Relative Gibbs free energies of different structural isomers involving the Zn<sup>2+</sup> cation and ligands *i*Pr-bpa or Me-bpa in the 1:2 ratio.<sup>a</sup>**

Complex cation	Isomer	GAS-PHASE							
		Mo5-2X	B3LYP	PBEo	BLYP	Mo6L	$\omega$ -B97XD	B97D3	B3LYP-D3
[Zn( <i>i</i> Pr-bpa) <sub>2</sub> ] <sup>2+</sup>	<i>cis-fac</i>	0.0	0.0	0.0	0.0	0.0	0.0	0.0	0.0
	<i>mer</i>	6.1	4.4	4.9	3.7	3.7	5.1	4.1	4.4
	<i>trans-fac</i>	6.7	4.7	5.0	4.1	5.2	6.3	5.3	5.6
[Zn(Me-bpa) <sub>2</sub> ] <sup>2+</sup>	<i>cis-fac</i>	0.0	1.5	1.2	1.5	0.0	0.0	0.0	0.0
	<i>mer</i>	0.7	0.0	0.0	0.0	1.4	0.1	0.7	0.6
	<i>trans-fac</i>	3.1	3.7	3.4	3.5	3.7	3.5	3.3	3.5
Complex cation	Isomer	ACETONITRILE SOLUTION							
		Mo5-2X	B3LYP	PBEo	BLYP	Mo6L	$\omega$ -B97XD	B97D3	B3LYP-D3
[Zn( <i>i</i> Pr-bpa) <sub>2</sub> ] <sup>2+</sup>	<i>cis-fac</i>	0.0	0.6	0.0	2.2	0.0	0.0	0.0	0.0
	<i>mer</i>	4.1	0.0	1.3	0.0	1.4	2.3	0.1	1.0
	<i>trans-fac</i>	5.9	4.3	4.2	5.2	3.7	5.3	4.0	4.5
[Zn(Me-bpa) <sub>2</sub> ] <sup>2+</sup>	<i>cis-fac</i>	0.9	3.3	2.5	3.4	1.3	0.6	0.2	0.4
	<i>mer</i>	0.0	0.0	0.0	0.0	0.0	0.0	0.0	0.0
	<i>trans-fac</i>	2.7	3.1	2.7	3.0	2.6	2.5	1.9	2.2

<sup>a</sup>All values are in kcal mol<sup>-1</sup>. The Gibbs free energies are obtained on the geometries optimized at the Mo5-2X/6-31+G(d)/LanL2DZ + ECP level of theory, with electronic energies attained as single-point calculations using the indicated DFT functional and the same basis sets. Solvent effects are modeled through the implicit SMD solvation.

B3LYP-D3. On the other hand, pure BLYP functional and its hybrid B3LYP analogue lean to give wrong trends, especially for [Zn(Me-bpa)<sub>2</sub>]<sup>2+</sup> in the gas-phase and [Zn(*i*Pr-bpa)<sub>2</sub>]<sup>2+</sup> in acetonitrile. Therefore, in what follows we will discuss the results pertaining the Mo5-2X functional, which is beneficial because it allows direct comparison with our earlier data.<sup>21,22</sup> The inspection of the calculated structures reveals that complexes of the *i*Pr-bpa derivative have a more distorted geometry than those of Me-bpa (Tables S6 and S7). In addition, the calculations show that the most stable geometrical isomer of [Zn(*i*Pr-bpa)<sub>2</sub>]<sup>2+</sup> is *cis-fac* in both the gas phase and acetonitrile solution, which is in accordance with the obtained crystal structure of **3<sub>Zn</sub>**. The prevalence of this isomer is retained for [Zn(Me-bpa)<sub>2</sub>]<sup>2+</sup> in the gas-phase, yet in acetonitrile *mer* becomes the most stable, which is consistently predicted with all tested DFT functionals. Nevertheless, for Me-bpa, the calculated energy differences among isomers were rather small, Table 2. In the literature, a number of [Zn(R-bpa)<sub>2</sub>]<sup>2+</sup> have been studied by single crystal X-ray diffraction. Interestingly, *cis-fac* isomers were found even for R-bpa complexes with a large substituent R on the amine nitrogen atom, where *trans-fac* would be expected due to steric crowding. This trend is also observed here, as the predominance of *mer* with a smaller R = Me changes to *cis-fac* with a larger R = *i*Pr. Additionally, *cis-fac* single crystal structures are known for derivatives with bulky R groups, including methyl ethanoate, *p*-chlorobenzyl and anthranil,<sup>43</sup> phenyl-triazole,<sup>44</sup> ferrocenyl,<sup>16</sup> methyl propanoate<sup>21</sup> and phatlimide.<sup>45</sup>

The complexes of diamagnetic Zn(II) were studied by NMR spectroscopy to give information about the formation of complexes in solution. The NMR spectra were recorded either of complexes prepared *in situ* in deuterated solvent or of complexes that were previously prepared in methanol, isolated and dissolved in deuterated solvent. As expected, the NMR spectra of previously isolated polymorphs **1a<sub>Zn</sub>** and **1b<sub>Zn</sub>** show presence of identical ML species **1<sub>Zn</sub>** at the NMR time-scale. Compared to the free ligand, the <sup>1</sup>H NMR spectrum of **1<sub>Zn</sub>** in CD<sub>3</sub>CN shows shifted peaks and broadening of the  $\alpha$ -CH<sub>2</sub> peak. The broad peak indicates a weak Zn-N bond at room temperature, which enables nitrogen inversion and equivalence of the  $\alpha$ -CH<sub>2</sub> protons. Strengthening of the

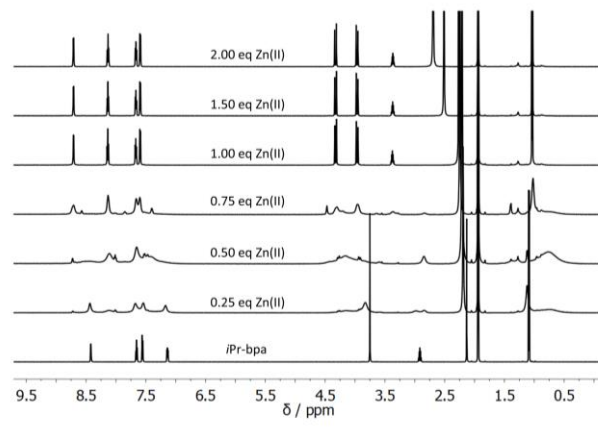
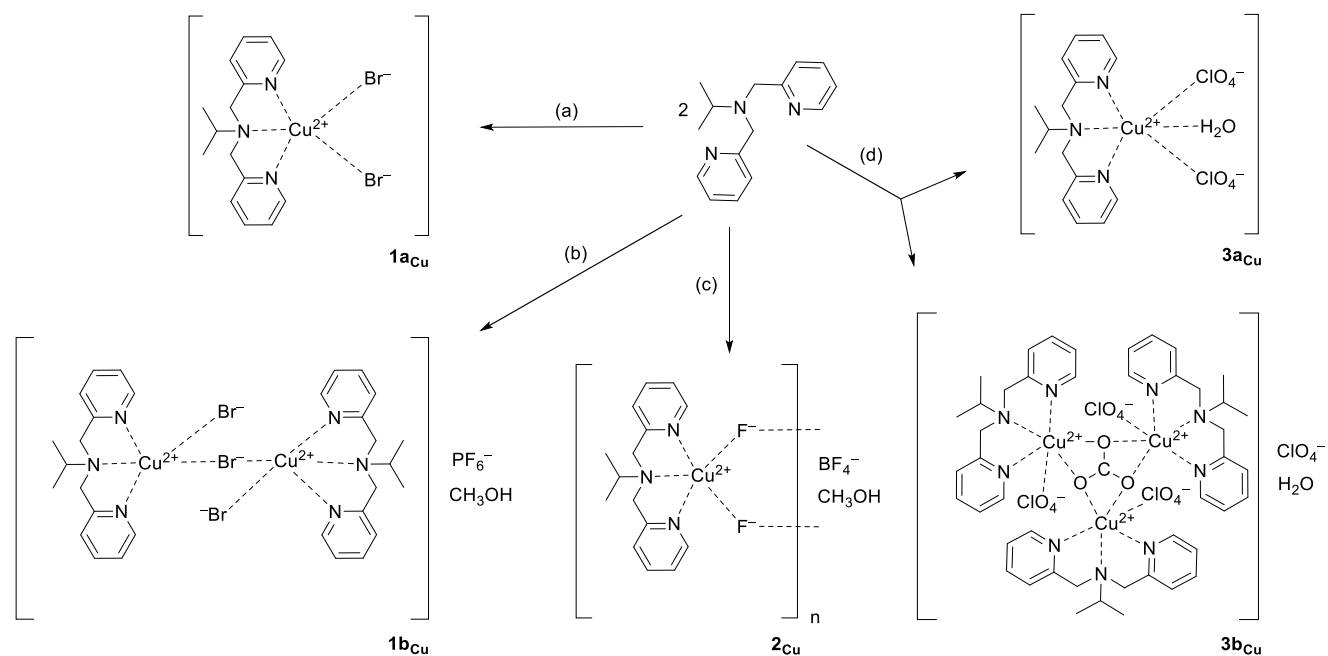


Figure 4. <sup>1</sup>H NMR (CD<sub>3</sub>CN) titration of *i*Pr-bpa with Zn(ClO<sub>4</sub>)<sub>2</sub>.

NMR study of Zn(II) complexes

Scheme 2. Synthesis of Cu(II) complexes<sup>a</sup>

<sup>a</sup>Reaction conditions: (a) CuBr<sub>2</sub>, methanol; (b) 2 CuBr<sub>2</sub>, 4 NH<sub>4</sub>PF<sub>6</sub>, methanol, (c) Cu(BF<sub>4</sub>)<sub>2</sub>, methanol; Cu(ClO<sub>4</sub>)<sub>2</sub>, (d) methanol, Cu(ClO<sub>4</sub>)<sub>2</sub>.

Zn–N bond was assumed to occur at lower temperatures and the <sup>1</sup>H NMR spectrum recorded at –40°C (Figure S24) shows splitting of the α-CH<sub>2</sub> peak into two doublets (4.36 and 4.12 ppm) with geminal coupling (*J* = 16 Hz), indicating a stronger bond and inhibited nitrogen inversion.<sup>21,22</sup>

The <sup>1</sup>H NMR spectrum of previously isolated **2**<sub>Zn</sub> shows a single species, possibly the bridged complex corresponding to the crystal structure. The NMR spectrum of the *in situ* prepared complex in a 2:1 ratio showed broad peaks (Figure S25), indicating an intermediate ligand exchange, similar as for complex **3**<sub>Zn</sub> at a 2:1 ratio (described later, Figure 4). These results show that in the previously isolated complex **2**<sub>Zn</sub>, there was enough fluoride ion to coordinate the Zn(II) and form a (bridged) ML complex, while in the *in situ* experiment, fluoride had not yet formed and it is likely a mixture of complexes with intermediate ligand exchange. When comparing the previously isolated **2**<sub>Zn</sub> and the *in situ* **iPr-bpa** and Zn(BF<sub>4</sub>)<sub>2</sub> in a 1:1 ratio, the spectra show slightly different chemical shifts. We assume that both complexes have ML stoichiometry, but the remaining coordination sites are occupied by F<sup>–</sup> anions in the isolated complex, and by acetonitrile molecules in the *in situ* experiment.

To describe the solution structure of **3**<sub>Zn</sub>, a <sup>1</sup>H NMR titration was performed (Figure 4), by adding Zn(ClO<sub>4</sub>)<sub>2</sub> to a solution of **iPr-bpa**. With the addition of 0.5 eq Zn(II), a ML<sub>2</sub> complex was expected to form, that would correspond to the solid state structure **3**<sub>Zn</sub>. However, the NMR spectrum showed broad signals, indicating an intermediate ligand exchange compared to the NMR timescale. By further adding Zn(II), a complex of ML stoichiometry is formed and remains the only species in solution for higher equivalents of Zn(II) (above 1 eq). Sharper signals of the ML complex indicate that the exchange is slower than the NMR timescale and the ML

complex more stable than ML<sub>2</sub>. Similar cases are described in literature<sup>22,44</sup>. The CD<sub>3</sub>CN solution of **iPr-bpa** and Zn(ClO<sub>4</sub>)<sub>2</sub> at a 2:1 ratio was cooled to –40°C in order to slow down the exchange. Sharpening of the signals was observed, but the many signals suggest a mixture of several species (Figure S27).

## Synthesis and characterization of Cu(II) complexes

Five complexes of **iPr-bpa** and Cu(II) were prepared using four different counterions (Scheme 2). Single crystal structures of two monomers **1a**<sub>Cu</sub> and **3a**<sub>Cu</sub>, a bridged dimer **1b**<sub>Cu</sub>, a coordination polymer **2**<sub>Cu</sub> and a cyclic trimer **3b**<sub>Cu</sub> were determined, their molecular structures are shown on Figures 5 and 6. Selected bond lengths are collected in Table 3.

Complex **1a**<sub>Cu</sub> was prepared using **iPr-bpa** and CuBr<sub>2</sub> in a 2:1 ratio. However, the crystal structure of **1a**<sub>Cu</sub> shows that due to coordination of bromide anions, a complex of ML stoichiometry was obtained, similarly as for previously described **1a**<sub>Zn</sub> / **1b**<sub>Zn</sub>. **1a**<sub>Cu</sub> is a penta-coordinated [CuBr<sub>2</sub>N<sub>3</sub>] complex of distorted square pyramidal geometry (*τ* = 0.33), where the ligand is bound meridionally [angle N<sub>1</sub>–Cu–N<sub>3</sub> 163.81(12)°, angle between pyridine planes = 8.56(18)°]. In the literature, a large number of penta-coordinated complexes *mer*-[CuX<sub>2</sub>(R-**bpa**)] are known.<sup>10,14,46,47</sup>

In the synthesis using **iPr-bpa**, CuBr<sub>2</sub> and NH<sub>4</sub>PF<sub>6</sub> in a ratio of 1:1:2, complex **1b**<sub>Cu</sub> was prepared. Unlike the Zn(II) complex **1b**<sub>Zn</sub> prepared in the same way, that was an ML monomer, the crystal structure of **1b**<sub>Cu</sub> reveals a complex of M<sub>2</sub>L<sub>2</sub> stoichiometry, where two pentacoordinated Cu(II) atoms are bridged by one bromide ion, [CuBrN<sub>3</sub>(μ-Br)CuN<sub>3</sub>]. Both Cu(II) have square pyramidal geometry (*τ* = 0.08, *τ*<sub>2</sub> = 0.28). The ligand is coordinated meridionally

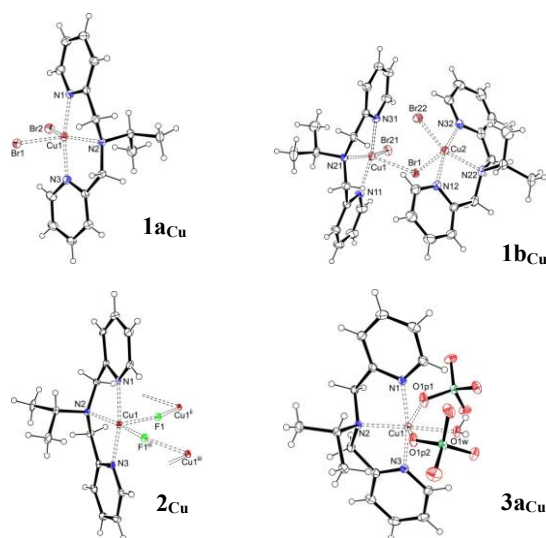


Figure 5. Molecular structures of complexes **1a<sub>Cu</sub>** ([Cu(*iPr*-bpa)Br<sub>2</sub>]), **1b<sub>Cu</sub>** ([Cu<sub>2</sub>(μ-Br)(Br)<sub>2</sub>(*iPr*-bpa)<sub>2</sub>](PF<sub>6</sub>) × CH<sub>3</sub>OH), **2<sub>Cu</sub>** ([Cu(μ-F)(*iPr*-bpa)]<sub>n</sub>(BF<sub>4</sub>)<sub>n</sub> × nCH<sub>3</sub>OH) and **3a<sub>Cu</sub>** ([Cu(*iPr*-bpa)(ClO<sub>4</sub>)<sub>2</sub>(H<sub>2</sub>O)]).

[angles Ni—Cu—N<sub>3</sub> 164.17(15)° and 164.56(17)°, angle between pyridine planes = 8.3(2)°, 8.7(3)°, respectively]. Similar bridged structures obtained by using the combination of halogen and PF<sub>6</sub><sup>−</sup> anions are described in literature.<sup>48</sup>

In the synthesis of **2<sub>Cu</sub>**, *iPr*-bpa and Cu(BF<sub>4</sub>)<sub>2</sub> were used in a 2:1 ratio. Similar as discussed for **2<sub>Zn</sub>**, decomposition of the BF<sub>4</sub><sup>−</sup> anion leads to the formation of fluoride ion. The crystal structure of **2<sub>Cu</sub>** showed that the F<sup>−</sup> ion acted as a bridging ligand, connecting the Cu(II) centers into a coordination polymer (ML)<sub>n</sub>. In **2<sub>Cu</sub>**, the Cu(II) center is penta-coordinated [Cu(μ-F)<sub>2</sub>N<sub>3</sub>]<sub>n</sub>, with an almost ideal square pyramidal geometry (τ = 0.03). The ligand in **2<sub>Cu</sub>** is bound meridionally [angle Ni—Cu—N<sub>3</sub> 167.0(2)°, and angle between pyridine planes = 1.1(3)°]. In the CSD database, only three halogenide bridged copper(II) coordination polymers with ligands structurally similar to bpa are published.<sup>49–51</sup>

In the synthesis using *iPr*-bpa and Cu(ClO<sub>4</sub>)<sub>2</sub> in a 2:1 ratio, two products with different crystal habits were obtained. The main product was hexagonal complex **3b<sub>Cu</sub>**, with a small amount of needle-like **3a<sub>Cu</sub>** crystals. The crystal structure of complex **3a<sub>Cu</sub>** shows a monomer of ML stoichiometry. The hexa-coordinated [CuO<sub>3</sub>N<sub>3</sub>] coordination polyhedron reveals a distorted octahedral geometry. Due to Jahn-Teller distortion, the axial bonds between Cu(II) and the perchlorate anions are elongated [2.5711(16) and 2.6875(14) Å] compared to the equatorial bonds [1.9652(18)–2.0429(14) Å]. The ligand is meridionally bound [angles Ni—Cu—N<sub>3</sub> 165.67(7)°, angle between pyridine planes = 7.23(10)°], and the remaining three coordination sites are occupied by two perchlorate anions and one water molecule. In the literature, two structures with a similar [Cu(*R*-bpa)(ClO<sub>4</sub>)<sub>2</sub>(H<sub>2</sub>O)] coordination sphere are known, namely with bpa ligands bearing anthranyl or guanidyl side chains.<sup>52</sup>

Surprisingly, complex **3b<sub>Cu</sub>** was found to capture atmospheric CO<sub>2</sub>. Due to the presence of water in the solvent as well as in the Cu(ClO<sub>4</sub>)<sub>2</sub> × 6H<sub>2</sub>O precursor and the basicity of the ligand, CO<sub>2</sub> was present in **3b<sub>Cu</sub>** in the form of carbonate ion. Several similar systems are described in literature.<sup>53–56</sup> In

**3b<sub>Cu</sub>**, the carbonate ion connects three Cu(II) centers, forming a cyclic trimer of C<sub>3</sub> molecular symmetry. Each Cu(II) is hexacoordinated, with a distorted octahedral geometry due to the bidentate binding of the carbonate ion. Three coordination sites in **3b<sub>Cu</sub>** are occupied by the ligand, two coordinated to the carbonate ion and one bound perchlorate anion, [Cu<sub>3</sub>(tri-μ-O)O<sub>3</sub>N<sub>9</sub>]. The ligand is a *mer* isomer [angles Ni—Cu—N<sub>3</sub> 166.4(3)°, angles between pyridine planes = 6.6(5)°].

The synthesis of **3b<sub>Cu</sub>** was repeated with bubbling CO<sub>2</sub> through the methanol solution of *iPr*-bpa and Cu(ClO<sub>4</sub>)<sub>2</sub> in a 2:1 ratio; phase purity of the obtained product was confirmed by X-ray powder diffraction (Figure S52). The attempts to prepare a higher yield of **3a<sub>Cu</sub>** in inert conditions, excluding water and/or air, were not successful.

Binding of CO<sub>2</sub> in the *iPr*-bpa / Cu(ClO<sub>4</sub>)<sub>2</sub> system was studied by UV-Vis spectroscopy. In basic solutions, CO<sub>2</sub> is present in the form of a carbonate ion so we assumed that the excess of ligand in the solution acted as a base. Two equivalents of *iPr*-bpa were added to Cu(ClO<sub>4</sub>)<sub>2</sub> in an acetonitrile solution, in an atmosphere of N<sub>2</sub>, then CO<sub>2</sub> was bubbled through the solution. For a 1:1 ligand to metal ratio, no significant change was observed. However, for the 2:1 ratio, binding of the carbonate ion caused a bathochromic shift, from 619 to 637 nm, corresponding to a similar carbonate bridged complex from literature (λ<sub>max</sub> = 639 nm).<sup>55</sup> These results indicate that an excess of ligand is necessary for the formation of the carbonate ion and carbonate bridged complex. It is interesting to note that in literature, similar Zn(II) complexes are studied as mimics of the enzyme carbonic anhydrase for binding of CO<sub>2</sub>.<sup>57–59</sup> In our case, CO<sub>2</sub> binding was observed only for the Cu(II) complex.

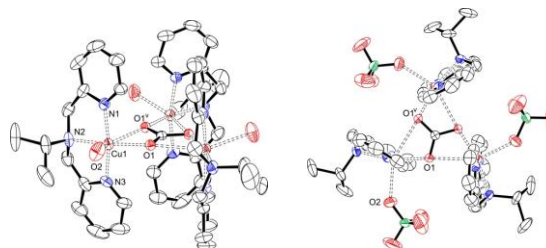


Figure 6. Molecular structure of complex **3b<sub>Cu</sub>** ([Cu<sub>3</sub>(tri-μ-CO<sub>3</sub>)(ClO<sub>4</sub>)<sub>3</sub>(*iPr*-bpa)<sub>3</sub>](ClO<sub>4</sub>)) viewed from two different perspectives; side view (left) and top view (right). Displacement ellipsoids were drawn at the 30% probability level. Perchlorate anions bound to Cu(II) ions were truncated from the structure (left) for better visibility of the ligand. In both views, the anions not bound to the metal

### Magnetic susceptibility of Cu(II) complexes

Magnetic susceptibility was measured for Cu(II) complexes **1a<sub>Cu</sub>**, **1b<sub>Cu</sub>**, **2<sub>Cu</sub>** and **3b<sub>Cu</sub>**. The susceptibility χ in Figure 7 monotonically increases with decreasing temperature from 300 K down to 2 K for all investigated copper complexes. The products χ · T at room temperature (inset in Figure 7) are 1.26 emu K/mol (**3b<sub>Cu</sub>**), 0.85 emu K/mol (**1b<sub>Cu</sub>**), and 0.42 emu K/mol (**2<sub>Cu</sub>** and **1a<sub>Cu</sub>**). Taking into account different number of copper ions in a molecule (three in **3b<sub>Cu</sub>**, two in **1b<sub>Cu</sub>**, and one in **2<sub>Cu</sub>** and **1a<sub>Cu</sub>**), the effective magnetic moment  $\mu_{eff} = \sqrt{8(\chi T)_{(per\ mol\ Cu)}}$  is 1.8 μ<sub>B</sub> for all four samples,<sup>60</sup>

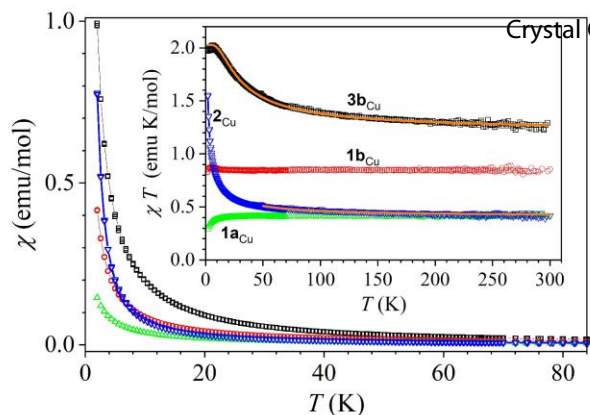


Figure 7. Temperature dependence of the susceptibility  $\chi$  and the product  $\chi \cdot T$  (inset). The full orange lines are fits as described in the main text.

where the constant  $\mu_B$  is the Bohr magneton. This value is in agreement with the expected value for Cu(II) ion with spin  $S=1/2$ .<sup>61</sup>

With decreasing temperature, the product  $\chi \cdot T$  remains more or less constant down to the lowest temperature for **1a<sub>Cu</sub>** and **1b<sub>Cu</sub>**. The result means there is no considerable magnetic interaction between magnetic moments in these two complexes. On the other hand, for **2<sub>Cu</sub>** and **3b<sub>Cu</sub>** the product  $\chi \cdot T$  starts to increase below approximately 100 K indicating ferromagnetic interactions between magnetic moments. Considering the structures of these two complexes we have estimated the interaction parameter  $J$  in the complexes.

In the polymer complex **2<sub>Cu</sub>** copper  $S=1/2$  ions form a quasi one dimensional structure and the interaction Hamiltonian can be written as a sum:

$$H = -J \sum_i \mathbf{S}_i \cdot \mathbf{S}_{i+1}. \quad (1)$$

For  $J > 0$  (a ferromagnetic interaction as in our case) no analytical equation has been proposed for  $\chi(T)$  calculated from the Hamiltonian (2).<sup>62</sup> A high-temperature series expansion was proposed in references 62 and 63. The fit of the experimental data above 50 K with the proposed rationale function from the reference<sup>62</sup> and  $g$ -factor 2.1, gave us the interaction parameter  $J = 12 \text{ cm}^{-1}$  (the full orange line in Figure 7 inset).

Table 3. Selected bond lengths (Å) for Cu(II) complexes.

Complex	Cu–N1 (Å)	Cu–N2 (Å)	Cu–N3 (Å)	Cu–anion or solvent (Å)
<b>1a<sub>Cu</sub></b>	2.004(3)	2.106(3)	1.979(3)	2.6254(6) (Br1); 2.4261(6) (Br2)
<b>1b<sub>Cu</sub></b>	2.015(4)	2.059(4)	1.996(4)	2.7341(7) (Br11); 2.4037(8) (Br21)
	1.992(4)	2.075(4)	1.981(4)	2.7341(7) (Br12); 2.3978(8) (Br22)
<b>2<sub>Cu</sub></b>	1.972(5)	2.043(5)	1.982(5)	2.282(3) (F1); 1.893(3) (F1 <sup>ii</sup> )
<b>3a<sub>Cu</sub></b>	1.9758(17)	2.0429(14)	1.9652(18)	2.5711(16) (O1p1); 2.6875(14) (O1p2)
				1.9777(13) (O1w, H <sub>2</sub> O)
				1.967(5) (O1, CO <sub>3</sub> <sup>-</sup> );
<b>3b<sub>Cu</sub></b>	1.956(5)	2.040(6)	1.963(5)	2.623(4) (O1 <sup>iii</sup> , CO <sub>3</sub> <sup>-</sup> )
				2.353(7) (O2, ClO <sub>4</sub> <sup>-</sup> )

In **3b<sub>Cu</sub>** the magnetic moments compose equilateral triangles with  $-\text{CO}_3^-$  unit as a bridge in the centre. Due to large distances between triangles, we assume only intramolecular interactions with an interaction Hamiltonian:

$$H = -J(\mathbf{S}_1 \cdot \mathbf{S}_2 + \mathbf{S}_1 \cdot \mathbf{S}_3 + \mathbf{S}_2 \cdot \mathbf{S}_3). \quad (2)$$

An excellent agreement between the experimental data and the susceptibility calculated from (1) using the PHI software<sup>64</sup> was obtained (full line in Figure 7 inset). The  $g$ -factor was set to 2.1 as the average value obtained from ESR, while the interaction parameter  $J = 19 \text{ cm}^{-1}$  was obtained as a result of the fitting procedure.

### ESR study of Cu(II) complexes

The ESR spectra of the investigated Cu(II) complexes, obtained at selected temperatures, are shown in Figure 8. The simulations were performed using EasySpin software.<sup>65</sup>

Considering the susceptibility results, for the simulation of the ESR spectra of complexes **1a<sub>Cu</sub>** and **1b<sub>Cu</sub>**, the following reduced form of spin-Hamiltonian was assumed:

$$H = \mu_B \mathbf{B} \mathbf{g} \mathbf{S} \quad (3)$$

For the polymer complex **2<sub>Cu</sub>**, the additional interaction term (1) was counted to (3). In Equation (3),  $\mathbf{B}$  is the external magnetic field,  $\mathbf{g}$  is the  $g$ -tensor and  $\mathbf{S}$  is the electron spin operator for the unpaired copper spin ( $S = 1/2$ ). The simulated spectra are shown in Figure 8 while the parameters used for the simulations are given in Table 4. The spectra were simulated using the same spin-Hamiltonian parameters in the whole temperature range, taking into consideration only the change of line-width of the assumed Lorentzian lines. All simulations were performed without using strain parameters. The spectra of complexes **1a<sub>Cu</sub>**, **1b<sub>Cu</sub>** and **2<sub>Cu</sub>** were simulated considering a rhombic  $g$ -tensor with three different  $g$ -values. No hyperfine lines, due to the interaction between electron ( $S = 1/2$ ) and nuclear spins ( $I = 3/2$ ), were detected. The simulations reproduce the experimentally observed spectra well (Figure 8).

The spectra of trimer complex **3<sub>Cu</sub>** were analyzed using the spin-Hamiltonian (3) expanded with an electron-electron interaction term:

$$H = -(\mathbf{S}_1 \cdot \mathbf{S}_2 + \mathbf{S}_1 \cdot \mathbf{S}_3 + \mathbf{S}_2 \cdot \mathbf{S}_3). \quad (4)$$

**Table 4: The values of spin-Hamiltonian parameters obtained from simulations. The calculated  $R$  parameter,<sup>70</sup> Addison structural parameters  $\tau^{23}$  and copper coordination geometries with RMSD value are also presented.<sup>69</sup>**

Compound	$S$	$g_1$	$g_2$	$g_3$	$D$	$R$ <sup>70</sup>	$\tau^{23}$	Coordination Geometry, RMSD <sup>69</sup>
<b>1a<sub>Cu</sub></b> (monomer)	1/2	2.075	2.210	2.235	-	5.400	0.33	trigonal bipyramid, 0.485
<b>1b<sub>Cu</sub></b> (dimer)	1/2	2.050	2.136	2.174	-	2.263	0.28, 0.08	distorted trigonal bipyramid, 0.540 square pyramid, 0.435
<b>2<sub>Cu</sub></b> (polymer)	1/2	2.060	2.135	2.175	-	1.875	0.03	square pyramid, 0.286
<b>3b<sub>Cu</sub></b> (trimer)	3/2	2.05	2.10	2.19	1.18 GHz	0.556	-	distorted octahedra, 0.635

Square pyramid:  $0 < \tau < 0.5$ , trigonal bipyramid  $0.5 < \tau < 1$ .

Contrary to Equation (2) where  $J$  describes the parameter of isotropic exchange interaction, here tensor  $\mathbf{J}_{tot}$  presents total interaction between three copper spins that includes the isotropic, antisymmetric (Dzyaloshinskii-Moriya) and symmetric interactions.<sup>66,67</sup> However, due the large number of parameters that have to be varied in the simulations, it is not straightforward to use Hamiltonian (4). Therefore, using the susceptibility study result that shows that copper ions in the triangular topology are coupled ferromagnetically with  $J = 19 \text{ cm}^{-1}$ , ESR simulations were performed assuming the total spin of the copper triangle  $S = 3/2$  and magnetic anisotropy described<sup>68</sup> by tensor  $\mathbf{D}$ :

$$\mathbf{H} = \mu_B \mathbf{B} \mathbf{g} \mathbf{S} + \mathbf{S} \mathbf{D} \mathbf{S} \quad (5)$$

From the obtained ESR simulation parameters given in Table 4, it is possible to correlate the copper coordination geometry<sup>23,69</sup> with the location of the unpaired electron.<sup>70</sup> A useful parameter is the value  $R = (g_2 - g_1)/(g_3 - g_2)$ . For parameter  $R$  larger than 1, the ground state of the unpaired electron is predominantly  $d_{z^2}$  while for  $R$  smaller than 1, the ground state is predominantly  $d_{x^2-y^2}$ .<sup>70</sup>

The spectra of the monomeric **1a<sub>Cu</sub>** complex have a so called "inverse" shape<sup>70</sup> and they can be simulated using  $g$ -

values  $g_2 \approx g_3 > g_1$ . These shapes are characteristic for trigonal bipyramidal complexes, in agreement with the observed coordination geometry, as could be seen from Table 4. The value of parameter  $R = 5.4$  reveals that the unpaired electron is predominantly in the  $d_{z^2}$  orbital. The nearest distance between two copper ions, determined from the crystal structure is  $7.321 \text{ \AA}$ , resulting in weak electron-electron interaction that leads to non-observance of hyperfine interaction in the spectra.<sup>4,47</sup>

Complex **1b<sub>Cu</sub>** with copper dimers shows one ESR line at all temperatures. The angle  $\text{Cu}_1\text{-Br}_2\text{-Cu}_2$  shown in Figure S39 is  $131.40^\circ$  and the shortest distance between copper ions in the dimer is  $4.954 \text{ \AA}$ . This copper arrangement is not favorable for the strong superexchange intra-dimer interaction, in line with the susceptibility results, confirmed also by the absence of half-field ESR transition.<sup>20</sup> However, the presence of weak exchange interaction between the copper ions could clearly be seen in the absence of two ESR signals from two non-equivalent copper ions in the unit cell but only one exchange narrowed line.<sup>19</sup>

In complex **2<sub>Cu</sub>**, the copper ions are arranged in a 1D zig-zag chain with the shortest distance between the copper ions

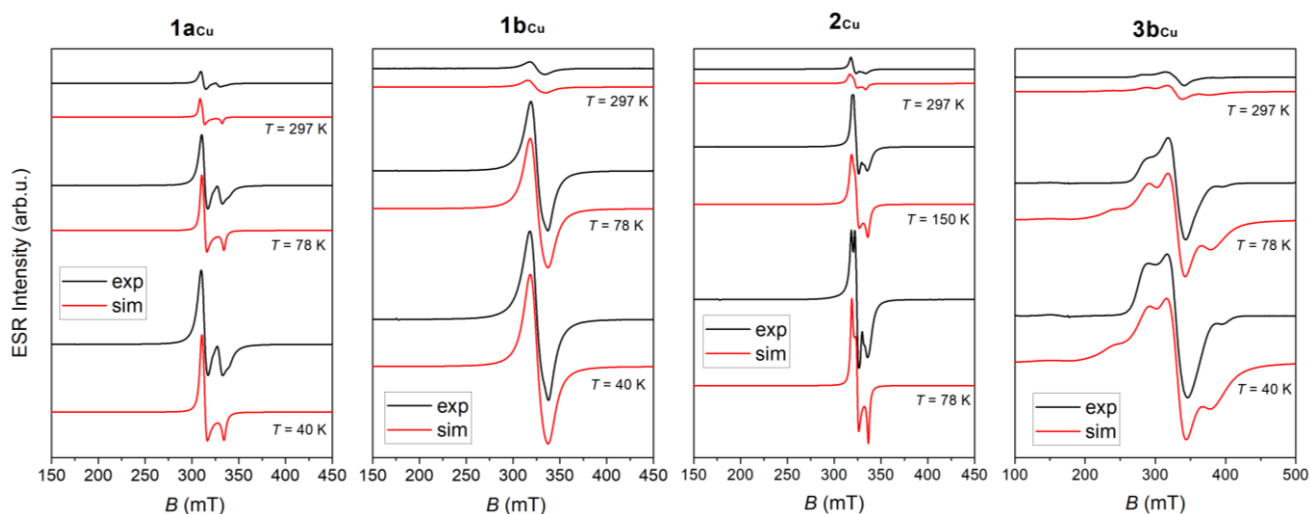


Figure 8. Experimental and simulated ESR spectra of the investigated complexes (from left to right, **1a<sub>Cu</sub>**, **1b<sub>Cu</sub>**, **2<sub>Cu</sub>**, **3b<sub>Cu</sub>**) at the indicated temperatures.

4.136 Å and Cu-F-Cu angle 164.22°. The ESR spectra are similar to the spectra of monomeric complex **1a<sub>Cu</sub>**. Adding the intra-chain exchange interaction term (i) to the spin-Hamiltonian (3) with the value of parameter  $J = 12 \text{ cm}^{-1}$  obtained from the susceptibility study does not influence the ESR patterns but only the line intensity. The simulations were tested for a different number of copper ions in the chain ( $N < 10$ ). The presence of spin-spin interaction is indicated by the absence of a hyperfine pattern in the ESR spectra.<sup>71</sup> The obtained value  $R = 1.875$  shows that the ground state of the unpaired electron is a combination of the  $d_{z^2}$  and  $d_{x^2-y^2}$  orbitals.<sup>70</sup>

From the spectral simulation of complex **3b<sub>Cu</sub>**, it could be concluded that using approximation (5) was justified. ESR study also confirms that the coupling in the triangle has to be ferromagnetic, in line with the magnetization study of similar tri-nuclear copper complexes.<sup>55,72,73</sup> Here, instead of using three copper spins with  $S = 1/2$  that interact through three equivalent superexchange pathways,<sup>55,73</sup> and Hamiltonian (4) the simulations were simplified using effective total spin of the triangle  $S = 3/2$  with small magnetic anisotropy described by zero-field splitting term  $D = 1.18 \text{ GHz} = 0.04 \text{ cm}^{-1}$ . In this rough approximation, the agreement between experimental and simulated spectra for complex **3b<sub>Cu</sub>** is satisfactory.

## Conclusions

This work describes late transition metal complexes of the **iPr-bpa** ligand featuring different coordination numbers, coordination geometry and stoichiometry depending on the metal ( $M = \text{Zn}^{2+}$  or  $\text{Cu}^{2+}$ ) and anion ( $A = \text{Br}^-$ ,  $\text{PF}_6^-$ ,  $\text{BF}_4^-$ ,  $\text{F}^-$  and/or  $\text{ClO}_4^-$ ), see Table 5.

Single crystal structures have been determined for all nine reported metal complexes. First, complexes **[M(bpa)Br<sub>2</sub>]** with **ML** stoichiometry were obtained in the reaction of **iPr-bpa** with **MBr<sub>2</sub>** salts, namely **1a<sub>Zn</sub>**, **1b<sub>Zn</sub>** and **1a<sub>Cu</sub>**. An attempt to incorporate the  $\text{PF}_6^-$  instead of the  $\text{Br}^-$  anion gave complex **1b<sub>Cu</sub>**, a single bridged **M<sub>2</sub>L<sub>2</sub>** dimer containing both  $\text{Br}^-$  and  $\text{PF}_6^-$ . Second, in the syntheses using the  $\text{BF}_4^-$  anion, fluoride ions were formed that coordinated to the metal. In the **M<sub>2</sub>L<sub>2</sub>** dimer **2<sub>Zn</sub>** two  $\text{F}^-$  counterions act as a double bridge, while the **(ML)<sub>n</sub>** polymer **2<sub>Cu</sub>** contains a single fluoride bridge. And third, using the perchlorate anion the **ML<sub>2</sub>**

complex **3<sub>Zn</sub>**, the cyclic **M<sub>3</sub>L<sub>3</sub>** complex **3b<sub>Cu</sub>** and a small quantity of the **ML** complex **3a<sub>Cu</sub>** were prepared. It is particularly interesting to mention that **3b<sub>Cu</sub>** was found to bind  $\text{CO}_2$  from the atmosphere in the form of carbonate, in a slightly basic solution due to the excess of free ligand.

The stability of polymorphs **1a<sub>Zn</sub>** and **1b<sub>Zn</sub>** was investigated by differential scanning calorimetry, hot-stage microscopy and X-ray powder diffraction. The diamagnetic zinc complexes have been studied in solution by NMR spectroscopy, for isolated complexes **1a<sub>Zn</sub>**/**1b<sub>Zn</sub>**, **2<sub>Zn</sub>** and **3<sub>Zn</sub>** as well as for complexes prepared *in situ* using different zinc / ligand ratios. The geometry and stability of different isomers of the **[Zn(iPr-bpa)<sub>2</sub>]<sup>2+</sup>** cation (*cis-fac*, *trans-fac* and *mer*) have been investigated by DFT calculations and compared to the experimentally obtained *cis-fac* **3<sub>Zn</sub>**. Magnetic susceptibility was measured and ESR spectra were recorded, simulated and analyzed for four copper complexes: the monomer **1a<sub>Cu</sub>**, the dimer **1b<sub>Cu</sub>**, the trimer **3b<sub>Cu</sub>** and coordination polymer **2<sub>Cu</sub>**.

Recently, we have reported on the synthesis and characterization of **[M(imda)<sub>2</sub>]<sup>2+</sup>** complexes,<sup>22</sup> that show a strong preference for *trans-fac* **ML<sub>2</sub>** complexes. Surprisingly, the rather similar **bpa** ligand presented herein showed (a) high coordination versatility (Table 5) and (b) if **[M(bpa)<sub>2</sub>]<sup>2+</sup>** complexes are formed, the preferred isomer is *cis-fac*. Therefore, careful design is necessary for the incorporation of **bpa** metal complexes in functional systems.

## Experimental

### General remarks

Reactions were carried out in ordinary glassware and chemicals were used as purchased from commercial suppliers without further purification. Synthesis of the ligand was carried out in a microwave reactor (CEM Discover), monitored by TLC on Aluminium oxide 60 F<sub>254</sub> neutral plates and detected with UV lamp (254 nm). Mass spectra were recorded on a HPLC-MS system (Agilent Technologies 1200) coupled with a 6410 Triple-Quadrupole mass spectrometer, operating in a positive ESI mode. The high-resolution mass spectra were obtained with a MALDI TOF/TOF instrument with  $\alpha$ -cyano-4-hydroxycinnamic acid (CHCA) as the matrix. NMR spectra were obtained on a Bruker Avance 300 or 600

**Table 5. Properties of Zn(II) and Cu(II) complexes of iPr-bpa.**

property	<b>1a<sub>Zn</sub></b>	<b>1b<sub>Zn</sub></b>	<b>2<sub>Zn</sub></b>	<b>3<sub>Zn</sub></b>	<b>1a<sub>Cu</sub></b>	<b>1b<sub>Cu</sub></b>	<b>2<sub>Cu</sub></b>	<b>3a<sub>Cu</sub></b>	<b>3b<sub>Cu</sub></b>
anion	$\text{Br}^-$	$\text{Br}^-$ , $\text{PF}_6^-$	$\text{BF}_4^-$ / $\text{F}^-$	$\text{ClO}_4^-$	$\text{Br}^-$	$\text{Br}^-$ , $\text{PF}_6^-$	$\text{BF}_4^-$ / $\text{F}^-$	$\text{ClO}_4^-$	$\text{ClO}_4^-$
coordination	$[\text{ZnBr}_2\text{N}_3]$	$[\text{ZnBr}_2\text{N}_3]$	$[\text{Zn}_2(\mu\text{-F})_2\text{N}_6]$	$[\text{ZnN}_6]$	$[\text{CuBr}_2\text{N}_3]$	$[\text{Cu}_2(\mu\text{-Br})\text{Br}_2\text{N}_6]$	$[\text{Cu}(\mu\text{-F})_2\text{N}_3]_n$	$[\text{CuO}_3\text{N}_3]$	$[\text{Cu}_3(\text{tri-}\mu\text{-O})\text{O}_3\text{N}_9]$
stoichiometry	ML	ML	<b>M<sub>2</sub>L<sub>2</sub></b>	<b>ML<sub>2</sub></b>	ML	<b>M<sub>2</sub>L<sub>2</sub></b>	<b>(ML)<sub>n</sub></b>	ML	<b>M<sub>3</sub>L<sub>3</sub></b>
CN	5	5	5	6	5	5	5	6	6
geometry	SP	TB / SP	TB	O	SP	SP	SP	O	O
isomer	<i>mer</i>	<i>fac</i>	<i>fac</i>	<i>cis-fac</i>	<i>mer</i>	<i>mer</i>	<i>mer</i>	<i>mer</i>	<i>mer</i>

Geometry classified according to the  $\tau$  parameter<sup>23</sup> and FindGeo program.<sup>69</sup> SP, TB and O are square pyramid, trigonal bipyramid and octahedron, respectively.

spectrometer, operating at 300 or 600 MHz for  $^1\text{H}$  and 75 or 150 MHz for  $^{13}\text{C}$ . The spectra are recorded at room temperature. Chemical shifts,  $\delta$  (ppm), indicate a downfield shift from the residual solvent signal ( $\delta_{\text{H}}$ : 1.94 ppm,  $\delta_{\text{C}}$ : 118.26 ppm,  $\text{CD}_3\text{CN}$ ). Coupling constants,  $J$ , are given in Hz. Infrared spectra were recorded using KBr pellets with a Bruker Alpha FT-IR spectrometer, in the 4000–350  $\text{cm}^{-1}$  region. The UV-Vis spectra were recorded on a Varian Cary 50 spectrophotometer using a 1 cm Suprasil quartz cell. The powder diffractograms were measured on a PANalytical Aeris instrument; conditions: Bragg-Brentano geometry ( $\theta$ - $2\theta$ ), source Cu-K $\alpha$  ( $\lambda=1.5418 \text{ \AA}$ ), measurement from  $5^\circ$  to  $70^\circ$  ( $2\theta$ ), with  $5.2^\circ/\text{min}$  ( $0.0216^\circ$  step and  $0.25 \text{ s/step}$ ). ESR study was performed using a Bruker Elexsys 580 FT/CW X-band spectrometer (microwave frequency 9.7 GHz). The spectra were recorded in the range from the room down to liquid helium temperature. Magnetic field modulation amplitude was 0.5 mT and modulation frequency was 100 kHz. The measurements were obtained on powder samples i.e. polycrystalline samples were grinded into powder. Dc susceptibility was measured with a Quantum Design MPMS-XL-5 magnetometer in a constant magnetic field of 1 kOe between 2 K and 300 K. All the presented data were corrected for the contribution of the sample holder and the diamagnetic susceptibility of inner shell electrons.<sup>74</sup> Differential Scanning Calorimetry (DSC) was carried out on a Perkin-Elmer Diamond. The sample cup was placed in the DSC apparatus together with an empty sample cup as a reference. Heating and cooling scans were recorded at a scan rate of  $10 \text{ }^\circ\text{C min}^{-1}$ . The phase transition temperatures were taken at the maximum of DSC transition peaks.

**Synthesis of N,N-Bis(pyrid-2-ylmethyl)-iso-propylamine (iPr-bpa).**<sup>21</sup> A mixture of isopropylamine (389  $\mu\text{L}$ , 4.6 mmol), 2-picolyl chloride hydrochloride (1.5 g, 9.1 mmol),  $\text{K}_2\text{CO}_3$  (6.3 g, 45.7 mmol) and KI (758.6 mg, 4.6 mmol) in acetonitrile (10 mL) was stirred in a round bottom flask equipped with a condenser in a microwave reactor (50 W, reflux) for 1 hour. The solvent was evaporated in a vacuum, the residue suspended in ethyl acetate and filtered. The filtrate was washed with saturated  $\text{NaHCO}_3$  and brine, the organic layer dried over anhydrous sodium sulfate, filtered and evaporated in a vacuum. The crude product was filtered under vacuum through a Büchner funnel, washed with water and dried in a vacuum. No further purification was required. Yield: 675.1 mg (2.8 mmol, 61%), brown powder,  $R_f = 0.38$ , neutral aluminium oxide, ethyl acetate:hexane = 3:7.  $^1\text{H NMR}$  (300 MHz,  $\text{CD}_3\text{CN}$ )  $\delta/\text{ppm}$ : 8.47 – 8.37 (m, 2H,  $\text{H}_{\text{Py-6}}$ ), 7.72–7.61 (m, 2H,  $\text{H}_{\text{Py-4}}$ ), 7.59 – 7.51 (m, 2H,  $\text{H}_{\text{Py-3}}$ ), 7.19 – 7.08 (m, 2H,  $\text{H}_{\text{Py-5}}$ ), 3.75 (s, 4H,  $\text{H}_\alpha$ ), 2.91 (hept,  $J = 6.6 \text{ Hz}$ , 1H,  $\text{H}_{\text{CH}}$ ), 1.09 (d,  $J = 6.6 \text{ Hz}$ , 6H,  $\text{H}_{\text{CH}_3}$ ).  $^{13}\text{C NMR}$  (75 MHz,  $\text{CD}_3\text{CN}$ )  $\delta/\text{ppm}$ : 162.16, 149.58, 137.17, 123.33, 122.64, 56.71, 51.21, 18.17.  $M_r(\text{C}_{15}\text{H}_{19}\text{N}_3) = 241.34$ . ESI-MS ( $m/z$ ): 264.1 ( $\text{M}+\text{Na}^+$ , 100%), 242.1 ( $\text{M}+\text{H}^+$ , 35%). MALDI-HRMS ( $m/z$ ): calcd 264.1471 [ $\text{C}_{15}\text{H}_{19}\text{N}_3 + \text{Na}^+$ ], found 264.1467. IR (KBr)  $\tilde{\nu}/\text{cm}^{-1}$ : 3452, 2964, 2876, 2835, 1591, 1567, 1474, 1435, 1180, 1048, 891, 770, 621, 550.

### Synthesis of metal complexes

Caution! Perchlorate salts of metal complexes with organic ligands are known to be explosive and should be handled with great caution and in small quantities. Therefore, thermal measurements were not performed for perchlorate complexes  $2\text{Zn}$ ,  $3\text{aCu}$  and  $3\text{bCu}$ .

**Method A.** Saturated methanol solutions of the ligand (1 or 2 eq) and metal salt (1 eq) were heated and boiled shortly in separate beakers until completely dissolved. The metal salt solution was added to the ligand solution and the mixture was cooled to room temperature and left partially covered for slow evaporation until crystals appeared (2 days to 2 months). The solvent was decanted and the crystals washed with diethyl ether (3 x 2 mL) and air-dried. Complexes that did not crystallize by method of slow evaporation were placed in a container with diethyl ether for slow diffusion.

**Method B.** To a chloroform solution (0.5 mL) of the ligand (2 eq) a solution of metal salt in methanol (2 mL) was slowly added. The bilayer solution was kept at  $4^\circ\text{C}$  and later at room temperature, partly covered for slow evaporation.

**mer-[Zn(iPr-bpa)Br<sub>2</sub>], 1a<sub>Zn</sub>.** iPr-bpa (17.26 mg, 0.072 mmol),  $\text{ZnBr}_2$  (8.05 mg, 0.036 mmol). Method A, the vial was placed in a screw capped container filled with diethyl-ether. After 2 weeks, crystals suitable for X-ray single crystal analysis were formed. Yield: 12.8 mg (0.027 mmol, 76%) of colorless cubic crystals. IR (KBr)  $\tilde{\nu}/\text{cm}^{-1}$ : 3442, 2966, 2928, 1605, 1592, 1477, 1441, 1165, 1048, 1019, 783, 770, 642, 620, 420.

**fac-[Zn(iPr-bpa)Br<sub>2</sub>], 1b<sub>Zn</sub>.** iPr-bpa (23.0 mg, 0.095 mmol),  $\text{ZnBr}_2$  (21.4 mg, 0.095 mmol),  $\text{NH}_4\text{PF}_6$  (31.0 mg, 0.190 mmol). Method A, the vial was placed in a screw capped container filled with diethyl-ether. After 5 days, crystals suitable for X-ray single crystal analysis were formed. Yield: 26.9 mg (0.058 mmol, 61%) of colorless plate-like crystals **1b<sub>Zn</sub>**. IR (KBr)  $\tilde{\nu}/\text{cm}^{-1}$ : 3453, 3065, 2975, 1607, 1422, 1088, 778, 647, 418.

Both polymorphs **1a<sub>Zn</sub>** and **1b<sub>Zn</sub>** have the same properties in solution. The dissolved complex is referred to as **1<sub>Zn</sub>**.  $^1\text{H NMR}$  (300 MHz,  $\text{CD}_3\text{CN}$ )  $\delta/\text{ppm}$ : 9.10 – 9.00 (m, 2H,  $\text{H}_{\text{Py-6}}$ ), 8.05 – 7.91 (m, 2H,  $\text{H}_{\text{Py-4}}$ ), 7.61 – 7.51 (m, 2H,  $\text{H}_{\text{Py-5}}$ ), 7.51–7.42 (m, 2H,  $\text{H}_{\text{Py-3}}$ ), 4.28 (s, 4H,  $\text{H}_\alpha$ ), 2.92 (hept,  $J = 6.7 \text{ Hz}$ , 1H,  $\text{H}_{\text{CH}}$ ), 0.89 (d,  $J = 6.7 \text{ Hz}$ , 6H,  $\text{H}_{\text{CH}_3}$ ).  $^{13}\text{C NMR}$  (75 MHz,  $\text{CD}_3\text{CN}$ )  $\delta/\text{ppm}$ : 155.99, 148.69, 141.19, 125.20, 124.20, 55.76, 53.12, 18.31. MALDI-HRMS ( $m/z$ ): calcd 384.0048 [ $\text{M}-\text{Br}^-$ ], found 384.0062.

**[Zn<sub>2</sub>( $\mu$ -F)<sub>2</sub>(iPr-bpa)<sub>2</sub>](BF<sub>4</sub>)<sub>2</sub>, 2z<sub>n</sub>.** iPr-bpa (40.2 mg, 0.166 mmol),  $\text{Zn}(\text{BF}_4)_2 \times \text{H}_2\text{O}$  (19.9 mg, 0.083 mmol). Method A, the vial was partly covered and left in the fume hood for slow evaporation for 2 days, then the vial was placed in a container with diethyl ether (10 mL) for diffusion for 8 days. Yield: 21.2 mg (0.03 mmol, 62%), yellow, needle-like crystals, suitable for X-ray single crystal analysis.  $^1\text{H NMR}$  (600 MHz,  $\text{CD}_3\text{CN}$ )  $\delta/\text{ppm}$ : 8.62 – 8.54 (m, 4H,  $\text{H}_{\text{Py-6}}$ ), 8.10 – 8.02 (m, 4H,  $\text{H}_{\text{Py-4}}$ ), 7.58 (d,  $J = 7.9 \text{ Hz}$ , 4H,  $\text{H}_{\text{Py-3}}$ ), 7.53 – 7.46 (m, 4H,  $\text{H}_{\text{Py-5}}$ ), 4.39 (d,  $J = 16.8 \text{ Hz}$ , 4H,  $\text{H}_\alpha$ ), 3.98 (d,  $J = 16.8 \text{ Hz}$ , 4H, 4H,  $\text{H}_\alpha$ ), 3.56 – 3.46 (m, 2H,  $\text{H}_{\text{CH}}$ ), 1.19 (d,  $J = 6.6 \text{ Hz}$ , 12H,  $\text{H}_{\text{CH}_3}$ ).  $^{13}\text{C NMR}$  (151 MHz,  $\text{CD}_3\text{CN}$ )  $\delta/\text{ppm}$ : 157.46, 148.89, 142.75, 125.95, 125.38, 57.37, 55.90, 18.76. MALDI-HRMS ( $m/z$ ): calcd 324.0849 [ $\text{M}-2\text{BF}_4^- - \text{F}^- - \text{Zn}^{2+} - \text{C}_{15}\text{H}_{19}\text{N}_3$ ], found 324.0867. IR (KBr)  $\tilde{\nu}/\text{cm}^{-1}$ : 3442, 2977, 1610, 1446, 1309, 1161, 1057, 770, 655, 522, 420.

**[Zn(iPr-bpa)<sub>2</sub>](ClO<sub>4</sub>)<sub>2</sub>, 3z<sub>n</sub>.** iPr-bpa (20.2 mg, 0.084 mmol),  $\text{Zn}(\text{ClO}_4)_2 \times 6\text{H}_2\text{O}$  (15.6 mg, 0.042 mmol). Method B, after 2 months, colorless plate-like crystals suitable for X-ray single crystal analysis were obtained. Yield: 8.41 mg (0.01 mmol, 27%).  $^1\text{H NMR}$  spectrum of **3z<sub>n</sub>** shows broad peaks and the peaks were therefore not assigned. MALDI-HRMS ( $m/z$ ): calcd 404.0350 [ $\text{M}-\text{ClO}_4^- - \text{C}_{15}\text{H}_{19}\text{N}_3$ ], found 404.0353. IR

(KBr)  $\tilde{\nu}/\text{cm}^{-1}$ : 3433, 3075, 2983, 1608, 1574, 1490, 1447, 1432, 1099, 797, 767, 623, 418.

[Cu(*iPr*-bpa)Br<sub>2</sub>]<sub>n</sub>, **1a**<sub>Cu</sub>. *iPr*-bpa (25.0 mg, 0.103 mmol), CuBr<sub>2</sub> (11.6 mg, 0.052 mmol). Method A, the vial was placed in a screw capped container filled with diethyl-ether. After 2 weeks, crystals suitable for X-ray single crystal analysis were formed. Yield: 9.5 mg (0.02 mmol, 39 %) of green cubic crystals. MALDI-HRMS (m/z): calcd 383.0053 [M-Br<sup>-</sup>], found 383.0051. IR (KBr)  $\tilde{\nu}/\text{cm}^{-1}$ : 3454, 2969, 1611, 1487, 1452, 1289, 1159, 1048, 781, 768, 655, 427.

[Cu<sub>2</sub>( $\mu$ -Br)(Br)<sub>2</sub>(*iPr*-bpa)<sub>2</sub>](PF<sub>6</sub>)<sub>2</sub> × CH<sub>3</sub>OH, **1b**<sub>Cu</sub>. *iPr*-bpa (22.4 mg, 0.093 mmol), CuBr<sub>2</sub> (20.7 mg, 0.093 mmol), NH<sub>4</sub>PF<sub>6</sub> (30.3 mg, 0.186 mmol). Method A, the vial was placed in a screw capped container filled with diethyl-ether. After 2 days, crystals suitable for X-ray single crystal analysis were formed. Yield: 30.7 mg (0.03 mmol, 64%) of blue-green needle-like crystals. MALDI-HRMS (m/z): calcd 383.0053 [M-2Br<sup>-</sup>-Cu<sup>2+</sup>-C<sub>15</sub>H<sub>19</sub>N<sub>3</sub>-PF<sub>6</sub><sup>-</sup>], found 383.0060. IR (KBr)  $\tilde{\nu}/\text{cm}^{-1}$ : 3444, 2975, 1611, 1451, 1288, 1154, 849, 749, 558.

[Cu( $\mu$ -F)(*iPr*-bpa)]<sub>n</sub>(BF<sub>4</sub>)<sub>n</sub> × nCH<sub>3</sub>OH, **2c**<sub>Cu</sub>. *iPr*-bpa (28.37 mg, 0.118 mmol), Cu(BF<sub>4</sub>)<sub>2</sub> × H<sub>2</sub>O (13.9 mg, 0.059 mmol). Method A, the vial was partly covered and left in the fume hood for slow evaporation for 2 days, then the vial was placed in a container with diethyl ether (10 mL) for diffusion for 2 days. Yield: 3.8 mg (0.01 mmol, 15%) blue, needle-like crystals, suitable for X-ray single crystal analysis. MALDI-HRMS (m/z): calcd 304.0864 [M-2F<sup>-</sup>-BF<sub>4</sub><sup>-</sup>], found 304.0863. IR (KBr)  $\tilde{\nu}/\text{cm}^{-1}$ : 3450, 2971, 2932, 1610, 1445, 1289, 1126, 1029, 746, 483.

[Cu(*iPr*-bpa)(ClO<sub>4</sub>)<sub>2</sub>(H<sub>2</sub>O)]<sub>n</sub>, **3a**<sub>Cu</sub>. *iPr*-bpa (18.1 mg, 0.075 mmol), Cu(ClO<sub>4</sub>)<sub>2</sub> × 6H<sub>2</sub>O (13.9 mg, 0.037 mmol). Method B, after 1 week, a small amount of blue needle-like ([Cu(*iPr*-bpa)(ClO<sub>4</sub>)<sub>2</sub>(H<sub>2</sub>O))] **3a**<sub>Cu</sub> and large amount of hexagonal ([Cu<sub>3</sub>(tri- $\mu$ -CO<sub>3</sub>)(ClO<sub>4</sub>)<sub>3</sub>(*iPr*-bpa)<sub>3</sub>)] **3b**<sub>Cu</sub> crystals, suitable for X-ray single crystal analysis were obtained.

[Cu<sub>3</sub>(tri- $\mu$ -CO<sub>3</sub>)(ClO<sub>4</sub>)<sub>3</sub>(*iPr*-bpa)<sub>3</sub>](ClO<sub>4</sub>)<sub>3</sub>, **3b**<sub>Cu</sub>. Method B, CO<sub>2</sub> was bubbled through the solution for 45 min, then the solution was left partly covered for slow evaporation. After 1 week, crystals suitable for X-ray single crystal analysis were formed. Yield: 7.1 mg (0.005 mmol, 36%) of blue hexagonal crystals. MALDI-HRMS (m/z): calcd 403.0355 [M-3ClO<sub>4</sub><sup>-</sup>-CO<sub>3</sub><sup>2-</sup>-2Cu<sup>2+</sup>-2 C<sub>15</sub>H<sub>19</sub>N<sub>3</sub>], found 403.0359. IR (KBr)  $\tilde{\nu}/\text{cm}^{-1}$ : 3441, 2975, 1610, 1445, 1121, 779, 765, 624, 425.

### Spectroscopic procedures

**NMR measurements (*in situ*).** Complexes were prepared by dissolving the ligand (0.5, 1 or 2 eq) and metal salt (1 eq) in approximately 0.6 mL CD<sub>3</sub>CN.

**NMR titration.** *iPr*-bpa (5.6 mg) was dissolved in 2 mL CD<sub>3</sub>CN (c(*iPr*-bpa) = 11.6 mM). Zn(ClO<sub>4</sub>)<sub>2</sub> × 6H<sub>2</sub>O (31.1 mg) was dissolved in 1 mL of the solution of *iPr*-bpa in CD<sub>3</sub>CN (c(Zn<sup>2+</sup>) = 83.6 mM), to avoid dilution. 600  $\mu$ L of the ligand solution was placed in an NMR tube and the spectrum of the free ligand was acquired. For each following measurement, an aliquot of the Zn<sup>2+</sup> in *iPr*-bpa solution was added until the ratio of Zn<sup>2+</sup>: *iPr*-bpa was 2:1.

**X-ray crystallography.** The X-ray intensity data were collected on an Oxford diffraction Xcalibur CCD diffractometer using monochromatic Cu-K $\alpha$  ( $\lambda = 1.54184$  Å) radiation. For temperature conditions see Tables S1 and S2. The data were

processed with CrysAlisPro program<sup>75</sup> (unit cell determination and data reduction). The structures were solved by direct methods with SIR2011 program<sup>76</sup> and refined against *F*<sup>2</sup> on all data by a full-matrix least squares procedure with SHELXL-97 program.<sup>77</sup> The monocrystalline samples diffracted up to  $\approx 76^\circ$  for all compounds except **3zn** for which the diffraction was observed up to  $\approx 62^\circ$ . This structure was solved by direct methods in the space group *Pna*<sub>2</sub>, with recognition of all non-hydrogen atoms. The central Zn atom from the cation and chlorine atoms from the perchlorate anions had positions in the vicinity of crystallographic glide planes of type *a* from space group *Pna*<sub>2</sub> (normal to the *b* axis). However, the significant residual density peaks were always present at the positions related to these glide planes imitating mirror symmetry with respect to the atoms from the starting model obtained by direct methods. Actually, during refinement in the space group *Pna*<sub>2</sub>, the significant number of systematic absence violations (66) related with this glide plane symmetry was observed. The model was tried to be refined with assumption of the twinning law (mirror symmetry perpendicular to the *b* axis), but without any improvement. Therefore, disordered models of complex cation and perchlorate anions were used in the final model for the refinement, where all atoms from individual disordered parts shared common occupancies. Perchlorate anions were modeled as rigid groups with oxygen atoms riding on the chlorine atoms having  $U_{\text{iso}} = 1.5 \times U_{\text{eq}}(\text{Cl})$ . Part of the complex cation with lower occupancy was restrained to have identical distances and angles as the part having higher occupancy (SAME instruction) and similar thermal parameters (SIMU and DELU instructions). All atoms with lower occupancy parts were refined in isotropic displacement parameter model. All hydrogen atoms were modeled as riding on carbon atoms on which they were bonded, without refinement of torsion angles. Due to lack of centers of inversion in space group *Pna*<sub>2</sub>, the final model also assumed racemic twinning as suggested by SHELXL program.<sup>77</sup> Such a model produced stable least-square refinements with a satisfying *R* value (6.89 %) and residual density at the level of the noise. Refined values for occupancies were: 0.887(3) and 0.113(3) for the complex cation; 0.587(12) and 0.413(12) for the first perchlorate anion in addition to 0.583(8) and 0.417(8) for the second perchlorate anion. Compound **3b**<sub>Cu</sub> was solved in trigonal space group *P-3c1* with recognition of all non-hydrogen atoms from the Cu trinuclear complex cation [(C<sub>15</sub>H<sub>19</sub>ClCuN<sub>3</sub>O<sub>5</sub>)<sub>3</sub>C]<sup>+</sup> lying on the three-fold symmetry axis. Such cation already binds three perchlorate units while one more perchlorate anion was located at two crystallographic positions of high symmetry (Wyckoff positions a and b).<sup>78</sup> Multiplicities of these Wyckoff positions are two times lower than multiplicities of Wyckoff positions of centers of Cu three-nuclear cations (Wyckoff positions d),<sup>78</sup> in accordance with stoichiometry of one perchlorate anion per one cation in the formula unit. High symmetries of perchlorate anion positions are not compatible with tetrahedral symmetry of the perchlorate anion, thus orientation disorder of perchlorate units is observed. Analogously with refinements of structure **3zn**, in refinements of **3b**<sub>Cu</sub>, perchlorate units were modeled as rigid group with oxygen atoms riding on the chlorine atoms with  $U_{\text{iso}} = 1.5 \times U_{\text{eq}}(\text{Cl})$ . All hydrogen atoms were modeled as riding on carbon atoms on which they were bonded, without refinement of torsion angles. Also, by inspection of intensity data, the possibility of 2-fold twinning

around  $b$  axis was observed. Addition of this twinning law significantly improved the  $R$  value. The precision of the determined C–C bonds was found to be somewhat lower than usual, presumably due to the twinning of the crystal and observed disorder of perchlorate anions. Racemic twinning was taken into account during refinements of compound  $2\text{Cu}$ , as suggested by program SHELXL.<sup>77</sup> This structure crystallizes in non-centrosymmetric space group  $P2_12_12_1$ , although non-chiral precursors were used in synthesis (crystallization resolution – conglomerates).<sup>79,80</sup> Counter anions like  $\text{ClO}_4^-$ ,  $\text{BF}_4^-$  or  $\text{PF}_6^-$  usually have large displacement parameters due to their high rotational freedom<sup>81</sup> and this is observed in the crystal structures of  $3\text{Zn}$ ,  $1\text{bCu}$ ,  $2\text{Cu}$  and  $3\text{bCu}$ . In the structure of  $1\text{bCu}$ , two solvent accessible voids of volume  $\approx 142 \text{ \AA}^3$  were observed with two peaks in the residual electron density. As the centers of these voids were located on crystallographic centers of inversion, the interpretation for these residual peaks as solvent molecules led to disorder because the symmetry related peaks were too close. Finally, the electron density from these regions was treated by SQUEZZE procedure in program PLATON<sup>82,83</sup> and final refinement model was performed without electron density contribution from this solvent accessible area. In all structures hydrogen atoms were positioned on calculated positions and refined within the riding model, having thermal parameters associated to carbon atoms on which they are bonded [ $U_{\text{iso}} = 1.5 \times U_{\text{eq}}(\text{C})$  for methyl groups and  $U_{\text{iso}} = 1.2 \times U_{\text{eq}}(\text{C})$  for all other hydrogen atoms]. Except for structures of  $3\text{Zn}$  and  $3\text{bCu}$ , additional refinements for torsional movement of methyl groups were included. Details for the X-ray diffraction studies are collected in Tables S1 and S2.

**Computational Details.** Structures of all investigated complexes were fully optimized employing the density functional theory (DFT) Mo5-2X/6-31+G(d)/LanL2DZ + ECP model, known to be successful in reproducing geometries, dipole moments and homolytic bond energies in various zinc complexes<sup>84,85</sup> and in line with our earlier reports.<sup>21,22</sup> In order to validate the quality of the selected methodology, the final electronic energies were obtained as single-point calculations using a range of DFT methods involving pure (BLYP, Mo6L), hybrid (B3LYP, PBE0), and dispersion-corrected ( $\omega$ -B97XD, B97D3, B3LYP-D3) functionals. Thermal corrections were extracted from the matching unscaled vibrational frequencies, so that all of the presented results correspond to differences in the total Gibbs free energies at a room temperature of 298 K and a normal pressure of 1 atm. To account for the effect of the acetonitrile solution, during geometry optimization we included the implicit SMD polarizable continuum solvation model, with all parameters for pure acetonitrile ( $\epsilon = 35.688$ ), being in line with our earlier reports.<sup>21,22</sup> All calculations were performed using the Gaussian 16 software.<sup>86</sup>

## ASSOCIATED CONTENT

### Supporting Information

Spectroscopic characterization of the ligand and complexes and Cartesian coordinates for all computed molecules. Crystallographic data is in cif format. CCDC 1966923-1966931. These data can be obtained free of charge from the Cambridge Crystallographic Data Centre via [www.ccdc.cam.ac.uk/data\\_request/cif](http://www.ccdc.cam.ac.uk/data_request/cif). For ESI see DOI: The

Supporting Information is available free of charge on the ACS Publications website.

## AUTHOR INFORMATION

### Corresponding Author

\*E-mail: Srecko.Kirin@irb.hr

### ORCID

Natalija Pantalon Juraj: 0000-0002-0357-5817  
 Senada Muratović: 0000-0001-5027-9191  
 Berislav Perić: 0000-0002-2397-2836  
 Nataša Šijaković Vujičić: 0000-0002-1455-9484  
 Robert Vianello: 0000-0003-1779-4524  
 Dijana Žilić: 0000-0003-2387-0853  
 Zvonko Jagličić: 0000-0002-4118-9677  
 Srećko I. Kirin: 0000-0002-0500-2422

### Conflicts of interest

There are no conflicts to declare.

### Acknowledgements

This work was supported by the Croatian Science Foundation (CSF, grants no. IP-2014-09-1461 and IP-2018-01-3168) and partially supported by the Slovenian Research Agency (Grant no. P2-0348).

### References

- Wende, C.; Lüdtke, C.; Kulak, N. Copper Complexes of N-Donor Ligands as Artificial Nucleases. *Eur. J. Inorg. Chem.* **2014**, *2014*, 2597–2612.
- Kirin, S. I.; Ott, I.; Gust, R.; Mier, W.; Weyhermüller, T.; Metzler-Nolte, N. Cellular Uptake Quantification of Metalated Peptide and Peptide Nucleic Acid Bioconjugates by Atomic Absorption Spectroscopy. *Angew. Chem. Int. Ed.* **2008**, *47*, 955–959.
- Berreau, L. M.; Saha, A.; Arif, A. M. Thioester Hydrolysis Reactivity of Zinc Hydroxide Complexes: Investigating Reactivity Relevant to Glyoxalase II Enzymes. *Dalton Trans.* **2006**, *1*, 183–192.
- Kirin, S. I.; Dübon, P.; Weyhermüller, T.; Bill, E.; Metzler-Nolte, N. Amino Acid and Peptide Bioconjugates of Copper(II) and Zinc(II) Complexes with a Modified N,N-Bis(2-picolyl)amine Ligand. *Inorg. Chem.* **2005**, *44*, 5495–5415.
- Zhang, Y.-P.; Ma, Z.-Y.; Gao, C.-Y.; Qiao, X.; Tian, J.-L.; Gu, W.; Liu, X.; Xu, J.-Y.; Zhao, J.-Z.; Yan, S.-P. Two Dpa-Based Zinc(II) Complexes as Potential Anticancer Agents: Nuclease Activity, Cytotoxicity and Apoptosis Studies. *New J. Chem.* **2016**, *40*, 7513–7521.
- Gao, C.-Y.; Qiao, X.; Ma, Z.-Y.; Wang, Z.-G.; Lu, J.; Tian, J.-L.; Xu, J.-Y.; Yan, S.-P. Synthesis, Characterization, DNA Binding and Cleavage, BSA Interaction and Anticancer Activity of Dinuclear Zinc Complexes. *Dalton Trans.* **2012**, *41*, 12220–12232.
- Carter, K. P.; Young, A. M.; Palmer, A. E. Fluorescent Sensors for Measuring Metal Ions in Living Systems. *Chem. Rev.* **2014**, *114*, 4564–4601.
- Zhu, L.; Yuan, Z.; Simmons, J. T.; Sreenath, K. Zn(II)-Coordination Modulated Ligand Photophysical Processes - the Development of Fluorescent Indicators for Imaging Biological Zn(II) Ions. *RSC Adv.* **2014**, *4*, 20398–20440.
- Hancock, R. D. The Pyridyl Group in Ligand Design for Selective Metal Ion Complexation and Sensing. *Chem. Soc.*

- Rev. **2013**, *42*, 1500–1524.
- (10) Ye, W.; Xiao, X.; Wang, L.; Hou, S.; Hu, C. Synthesis of Mono- and Binuclear Cu(II) Complexes Bearing Unsymmetrical Bipyridine–Pyrazole–Amine Ligand and Their Applications in Azide–Alkyne Cycloaddition. *Organometallics* **2017**, *36*, 2116–2125.
- (11) Tordin, E.; List, M.; Monkowius, U.; Schindler, S.; Knör, G. Synthesis and Characterisation of Cobalt, Nickel and Copper Complexes with Tripodal 4N Ligands as Novel Catalysts for the Homogeneous Partial Oxidation of Alkanes. *Inorg. Chim. Acta* **2013**, *402*, 90–96.
- (12) Barsoum, D. N.; Kyeremeh-Mensah, L.; Meisner, Q. J.; Clark, R. J.; Masson, E.; Zhu, L. Zinc(II) Complexes of N,N-Di(2-picolyl)hydrazones. *Eur. J. Inorg. Chem.* **2016**, *2016*, 5477–5484.
- (13) van der Salm, H.; Elliott, A. B. S.; Gordon, K. C. Substituent Effects on the Electronic Properties of Complexes with Dipyrindophenazine and Triazole Ligands: Electronically Connected and Disconnected Ligands. *Coord. Chem. Rev.* **2015**, *282–283*, 33–49.
- (14) Nielsen, A.; Veltzé, S.; Bond, A. D.; McKenzie, C. J. Isomerism in Copper(II) Chloride Complexes of Bis(2-Pyridylmethyl)Amine and N-Substituted Derivatives: Synthesis and X-Ray Structural Characterisation. *Polyhedron* **2007**, *26*, 1649–1657.
- (15) Wang, Y.; Liu, H.; Zhang, X.; Zhang, Z.; Huang, D. Experimental and Mechanistic Insights into Copper(II)–Dioxygen Catalyzed Oxidative N-Dealkylation of N-(2-pyridylmethyl)phenylamine and its Derivatives. *Org. Biomol. Chem.* **2017**, *15*, 9164–9168.
- (16) Maity, B.; Gadadhar, S.; Goswami, T. K.; Karande, A. A.; Chakravarty, A. R. Impact of Metal on the DNA Photocleavage Activity and Cytotoxicity of Ferrocenyl Terpyridine 3d Metal Complexes. *Dalton Trans.* **2011**, *40*, 11904–11913.
- (17) Velusamy, M.; Palaniandavar, M.; Justin Thomas, K. R. Cis-Facial Coordination of Bis(pyrid-2-ylmethyl)amine (Bpma). Synthesis, Structure and Spectral Behaviour of  $[\text{Ni}(\text{Bpma})_2]^{2+}$ . *Polyhedron* **1998**, *17*, 2179–2186.
- (18) Park, B. K.; Lee, S. H.; Lee, E. Y.; Kwak, H.; Lee, Y. M.; Lee, Y. J.; Jun, J. Y.; Kim, C.; Kim, S.-J.; Kim, Y. Zinc(II) Polymeric Compounds with a Chelating Ligand Bis(2-pyridylmethyl)amine (Bispicam) Directed by Intermolecular C/N/O–H...X (X=Cl, Br, I) Interactions: Catalytic Activities. *J. Mol. Struct.* **2008**, *890*, 123–129.
- (19) Žilić, D.; Rakvin, B.; Milić, D.; Pajić, D.; Đilović, I.; Cametti, M.; Džolić, Z. Crystal Structures and Magnetic Properties of a Set of Dihalo-Bridged Oxalamidato Copper(II) Dimers. *Dalton Trans.* **2014**, *43*, 11877–11887.
- (20) Manzur, J.; Vega, A.; García, A. M.; Acuña, C.; Sieger, M.; Sarkar, B.; Niemeyer, M.; Lissner, F.; Schleid, T.; Kaim, W. Coordination Alternatives in Dinuclear Bis(pyridin-2-ylalkyl)-benzylaminecopper(II) Complexes with OH-, RO-, F-, or Cl- Bridges: Experimental Structures and DFT Preferences. *Eur. J. Inorg. Chem.* **2007**, *9*, 5500–5510.
- (21) Škalamera, Đ.; Sanders, E.; Vianello, R.; Maršavelski, A.; Pevec, A.; Turel, I.; Kirin, S. I. Synthesis and Characterization of ML and ML<sub>2</sub> Metal Complexes with Amino Acid Substituted Bis(2-picolyl)amine Ligands. *Dalton Trans.* **2016**, *45*, 2845–2858.
- (22) Pantalon Juraj, N.; Miletić, G.; Perić, B.; Popović, Z.; Smrečki, N.; Vianello, R.; Kirin, S. I. Stereochemistry of Hexacoordinated Zn(II), Cu(II), Ni(II) and Co(II) Complexes with Iminodiacetamide Ligands. *Inorg. Chem.* **2019**, *58*, 16445–16457.
- (23) Addison, A. W.; Rao, T. N.; Reedijk, J.; van Rijn, J.; Verschoor, G. C. Synthesis, Structure, and Spectroscopic Properties of Copper(II) Compounds Containing Nitrogen-Sulphur Donor Ligands; the Crystal and Molecular Structure of Aqua[1,7-bis(N-methylbenzimidazol-2'-yl)-2,6-dithiaheptane]copper(II) Perchlorate. *J. Chem. Soc. Dalton Trans.* **1984**, *7*, 1349–1356.
- (24) Plenio, H.; Burth, D. Aminoferrocenes and Aminocobaltocenes as Redox-Active Chelating Ligands: Syntheses, Structures, and Coordination Chemistry. *Organometallics* **1996**, *15*, 4054–4062.
- (25) Abufarag, A.; Vahrenkamp, H. Zinc Complexes of the Ligand Dipicolylglycine. *Inorg. Chem.* **1995**, *34*, 2207–2216.
- (26) Štefane, B.; Perdih, F.; Višnjevac, A.; Požgan, F. Novel Triazole-Based Ligands and Their Zinc(II) and Nickel(II) Complexes with a Nitrogen Donor Environment as Potential Structural Models for Mononuclear Active Sites. *New J. Chem.* **2015**, *39*, 566–575.
- (27) Theodora Mphure, L.; Visser, H.; Roodt, A.; Brink, A. Crystal Structure of Dichloro-N,N-bis(pyridine-2-ylmethyl)cyclohexamino copper(II), C<sub>18</sub>H<sub>23</sub>Cl<sub>2</sub>CuN<sub>3</sub>. *Z. Krist. NCS* **2015**, *230*, 156–158.
- (28) Carreira-Barral, I.; Rodríguez-Blas, T.; Platas-Iglesias, C.; Blas, A.; Esteban-Gómez, D. Cooperative Anion Recognition in Copper(II) and Zinc(II) Complexes with a Ditopic Tripodal Ligand Containing a Urea Group. *Inorg. Chem.* **2014**, *53*, 2554–2568.
- (29) Song, Y.; Kim, D.; Lee, H.-J.; Lee, H. Synthesis and Structural Characterization of [(Dpca)MX<sub>2</sub>] (M=Cu, X=Cl; M=Cd, X=Br and M=Zn, X=NO<sub>3</sub>) Complexes Containing N,N-Di(2-picolyl)cyclohexylamine (Dpca) and Their Application to Methyl Methacrylate Polymerization. *Inorg. Chem. Commun.* **2014**, *45*, 66–70.
- (30) Mikata, Y.; Fujimoto, T.; Fujiwara, T.; Kondo, S. Intramolecular Ether Oxygen Coordination in the Zinc Complexes with Dipicolylamine (DPA)-Derived Ligands. *Inorg. Chim. Acta* **2011**, *370*, 420–426.
- (31) Gavezzotti, A.; Filippini, G. Polymorphic Forms of Organic Crystals at Room Conditions: Thermodynamic and Structural Implications. *J. Am. Chem. Soc.* **1995**, *117*, 12299–12305.
- (32) Leitão, M. L. P.; Canotilho, J.; Cruz, M. S. C.; Pereira, J. C.; Sousa, A. T.; Redinha, J. S. Study of Polymorphism From DSC Melting Curves; Polymorphs of Terfenadine. *J. Therm. Anal. Calorim.* **2002**, *68*, 397–412.
- (33) van den Ende, J. A.; Ensing, B.; Cuppen, H. M. Energy Barriers and Mechanisms in Solid–Solid Polymorphic Transitions Exhibiting Cooperative Motion. *CrystEngComm* **2016**, *18*, 4420–4430.
- (34) Saihara, K.; Yoshimura, Y.; Fujimoto, H.; Shimizu, A. Detrimental Effect of Glass Sample Tubes on Investigations of BF<sub>4</sub><sup>-</sup>-Based Room Temperature Ionic Liquid–Water Mixtures. *J. Mol. Liq.* **2016**, *219*, 493–496.
- (35) Casellas, H.; Pevec, A.; Kozlevčar, B.; Gamez, P.; Reedijk, J. An Unprecedented M<sub>4</sub>-SiF<sub>6</sub><sup>2-</sup>-Bridged Supramolecular Polymer Consisting of Bis-μ-F-Bridged Dinuclear Cu(II) Dications. *Polyhedron* **2005**, *24*, 1549–1554.
- (36) Lee, S. C.; Holm, R. H. Fluoride-Bridged Dimers: Binuclear Copper(II) Complexes and Iron(III)-Copper(II) Assemblies. *Inorg. Chem.* **1993**, *32*, 4745–4753.
- (37) Gobeze, W. A.; Milway, V. A.; Moubarak, B.; Murray, K. S.; Brooker, S. Solvent Control: Dinuclear versus Tetranuclear Complexes of a Bis-Tetradentate Pyrimidine-Based Ligand. *Dalton Trans.* **2012**, *41*, 9708–9721.
- (38) Dammers, S.; Zimmermann, T. P.; Walleck, S.; Stämmler, A.; Bögge, H.; Bill, E.; Glaser, T. A Mixed-Valence Fluorido-Bridged Fe<sup>II</sup>Fe<sup>III</sup> Complex. *Inorg. Chem.* **2017**, *56*, 1779–1782.
- (39) Inomata, M.; Suenaga, Y. Crystal Structure of a Dinuclear Co<sup>II</sup> Complex with Bridging Fluoride Ligands: Di-μ-fluorido-bis[tris[(6-methylpyridin-2-yl)methyl]amine]dicobalt(II) bis(tetrafluoroborate). *Acta Crystallogr. Sect. E. Struct. Rep. Online* **2014**, *70*, m359–m360.
- (40) Olguín, J.; Kalisz, M.; Clérac, R.; Brooker, S. Di- and Tetranuclear Copper(II), Nickel(II), and Cobalt(II) Complexes of Four Bis-Tetradentate Triazole-Based Ligands: Synthesis, Structure, and Magnetic Properties. *Inorg. Chem.* **2012**, *51*,

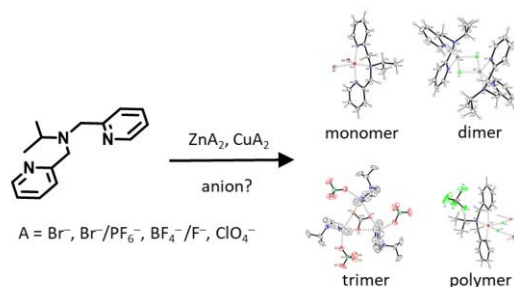
- 5058–5069.
- (41) Zang, Y.; Jang, H. G.; Chiou, Y.-M.; Hendrich, M. P.; Que, L. Structures and Properties of Ferromagnetically Coupled Bis( $\mu$ -halo)diiron(II) Complexes. *Inorg. Chim. Acta* **1993**, *213*, 41–48.
- (42) Jacobson, R. R.; Tyeklar, Z.; Karlin, K. D.; Zubieta, J. Fluoride as a Terminal and Bridging Ligand for Copper: Isolation and x-Ray Crystallographic Characterization of Copper Monomeric and Dimeric Complexes [Cu<sup>II</sup>(TMPA)F]<sub>n</sub><sup>+</sup> (n = 1 or 2; TMPA = Tris[(2-pyridyl)methyl]amine). *Inorg. Chem.* **1991**, *30*, 2035–2040.
- (43) Simmons, J. T.; Yuan, Z.; Daykin, K. L.; Nguyen, B. T.; Clark, R. J.; Shatruk, M.; Zhu, L. Bis[ N -alkyl- N N -di(2-pyridylmethyl)amine]zinc(II) Perchlorates Display Cis-Facial Stereochemistry in Solid State and Solution. *Supramol. Chem.* **2014**, *26*, 214–222.
- (44) Simmons, J. T.; Allen, J. R.; Morris, D. R.; Clark, R. J.; Levenson, C. W.; Davidson, M. W.; Zhu, L. Integrated and Passive 1,2,3-Triazolyl Groups in Fluorescent Indicators for Zinc(II) Ions: Thermodynamic and Kinetic Evaluations. *Inorg. Chem.* **2013**, *52*, 5838–5850.
- (45) Bantia, S.; Samanta, A. Multiple Logical Access with a Single Fluorophore–Spacer–Receptor System: Realization of Inhibit (INH) Logic Function. *Eur. J. Org. Chem.* **2005**, *23*, 4967–4970.
- (46) Colomban, C.; Martin-Diaconescu, V.; Parella, T.; Goeb, S.; García-Simón, C.; Lloret-Fillol, J.; Costas, M.; Ribas, X. Design of Zn-, Cu-, and Fe-Coordination Complexes Confined in a Self-Assembled Nanocage. *Inorg. Chem.* **2018**, *57*, 3529–3539.
- (47) Evans, A. J.; Watkins, S. E.; Craig, D. C.; Colbran, S. B. Copper Complexes with Ferrocenyl Pendants: Evidence for an Fe<sup>II</sup> ~ Cu<sup>II</sup>  $\rightleftharpoons$  Fe<sup>III</sup> ~ Cu<sup>I</sup> Electron Transfer Equilibrium Leading to a Reaction with Dioxygen. *J. Chem. Soc. Dalton Trans.* **2002**, *6*, 983–994.
- (48) Antonioli, B.; Büchner, B.; Clegg, J. K.; Gloe, K.; Gloe, K.; Götzke, L.; Heine, A.; Jäger, A.; Jolliffe, K. A.; Kataeva, O.; Kataev, V.; Klingeler, R.; Krause, T.; Lindoy, L. F.; Popa, A.; Seichter, W.; Wenzel, M. Interaction of an Extended Series of N-Substituted Di(2-picolyl)amine Derivatives with Copper(II). Synthetic, Structural, Magnetic and Solution Studies. *Dalton Trans.* **2009**, *24*, 4795–4805.
- (49) Abdi, K.; Hadadzadeh, H.; Weil, M.; Rudbari, H. A. Mono- and Polynuclear Copper(II) Complexes Based on 2,4,6-Tris(2-pyridyl)-1,3,5-triazine and its Hydrolyzed Form. *Inorg. Chim. Acta* **2014**, *416*, 109–121.
- (50) Cao, M.-L. Catena-poly[[[4,6-bis-(2-pyrid-yl)-1,3,5-triazin-2-olato]copper(II)]- $\mu$ -chlorido]. *Acta Crystallogr. Sect. E. Struct. Rep. Online* **2011**, *67*, m739–m739.
- (51) Folgado, J. V.; Coronado, E.; Beltrán-Porter, D.; Burriel, R.; Fuertes, A.; Miravittles, C. Crystal Structures and Magnetic Properties of the Mono- $\mu$ -Halogeno-Bridged Copper(II) Chains Cu(Pcpci)X [Pcpci = N-(2'-Pyridylcarbonyl)pyridine-2-carboximidate, X = Cl or Br]. *J. Chem. Soc. Dalton Trans.* **1988**, *12*, 3041–3045.
- (52) Belousoff, M. J.; Tjioe, L.; Graham, B.; Spiccia, L. Synthesis, X-Ray Crystal Structures, and Phosphate Ester Cleavage Properties of Bis(2-pyridylmethyl)amine Copper(II) Complexes with Guanidinium Pendant Groups. *Inorg. Chem.* **2008**, *47*, 8641–8651.
- (53) Muthuramalingam, S.; Khamrang, T.; Velusamy, M.; Mayilmurugan, R. Catalytic Fixation of Atmospheric Carbon Dioxide by Copper(II) Complexes of Bidentate Ligands. *Dalton Trans.* **2017**, *46*, 16065–16076.
- (54) Liu, H.-X.; Zhang, X.; Gao, X.-J.; Chen, C.; Huang, D. Synthesis and Mechanism Study of a Dimeric Tetranuclear Carbonate-Bridged Copper(II) Complex Resulting from CO<sub>2</sub> Fixation by Controlling O<sub>2</sub> Concentration. *Inorg. Chem. Commun.* **2016**, *68*, 63–67.
- (55) Massoud, S. S.; Louka, F. R.; Al-Hasan, M. A.; Vicente, R.; Mautner, F. A. Magneto-Structural Properties of Carbonate-Bridged Copper(II) Complexes: Fixation of Atmospheric CO<sub>2</sub>. *New J. Chem.* **2015**, *39*, 5944–5952.
- (56) Kolks, G.; Lippard, S. J.; Waszczak, J. V. A Tricopper(II) Complex Containing a Triply Bridging Carbonate Group. *J. Am. Chem. Soc.* **1980**, *102*, 4832–4833.
- (57) Arstad, B.; Blom, R.; Didriksen, T.; Frøseth, M.; Heyn, R. H.; Øien-Ødegaard, S. NMR Spectroscopic Investigations into the Mechanism of Absorption and Desorption of CO<sub>2</sub> by (Tris-pyridyl)amine Zn Complexes. *J. CO<sub>2</sub> Util.* **2017**, *19*, 58–67.
- (58) Liu, X.; Du, P.; Cao, R. Trinuclear Zinc Complexes for Biologically Relevant Mu<sub>3</sub>-Oxoanion Binding and Carbon Dioxide Fixation. *Nat. Commun.* **2013**, *4*, 2375.
- (59) Murthy, N. N.; Karlin, K. D. A Dinuclear Zinc Hydroxide Complex Which Traps Atmospheric Carbon Dioxide: Formation of a Tri-Zinc Complex with a Triply Bridging Carbonate Group. *J. Chem. Soc. Chem. Commun.* **1993**, *15*, 1236–1238.
- (60) Mabbs, F. E.; Machin, D. J. *Magnetism and Transition Metal Complexes*; Dover Publications, Inc. Mineola, New York, **1973**.
- (61) Ashcroft, N. W.; Mermin, N. D. *Solid State Physics*; Saunders College Publishing, USA, **1976**.
- (62) Kahn, O. *Molecular Magnetism*; VCH Publishing, **1993**.
- (63) Baker, G.; Rushbrooke, G.; Gilbert, H. High-Temperature Series Expansions for the Spin 1/2 Heisenberg Model by the Method of Irreducible Representations of the Symmetric Group. *Phys. Rev.* **1964**, *135*, 1272–1277.
- (64) Chilton, N. F.; Anderson, R. P.; Turner, L. D.; Soncini, A.; Murray, K. S. PHI: A Powerful New Program for the Analysis of Anisotropic Monomeric and Exchange-Coupled Polynuclear d- and f-Block Complexes. *J. Comput. Chem.* **2013**, *34*, 1164–1175.
- (65) Stoll, S.; Schweiger, A. EasySpin, a Comprehensive Software Package for Spectral Simulation and Analysis in EPR. *J. Magn. Reson.* **2006**, *178*, 42–55.
- (66) www.easyspin.org.
- (67) Ferrer, S.; Lloret, F.; Pardo, E.; Clemente-Juan, J. M.; Liu-González, M.; García-Granda, S. Antisymmetric Exchange in Triangular Tricopper(II) Complexes: Correlation among Structural, Magnetic, and Electron Paramagnetic Resonance Parameters. *Inorg. Chem.* **2012**, *51*, 985–1001.
- (68) Yurtaeva, S. V.; Gilmudtinov, I. F.; Rodionov, A. A.; Zaripov, R. B.; Kutyreva, M. P.; Bondar, O. V.; Nedopekin, O. V.; Khafizov, N. R.; Kadkin, O. N. Ferromagnetically Coupled Copper(II) Clusters Incorporated in Functionalized Boltorn H30 Hyperbranched Polymer Architecture: ESR, Magnetic Susceptibility Measurements, and Quantum-Chemical Calculations. *ACS Omega* **2019**, *4*, 16450–16461.
- (69) Andreini, C.; Cavallaro, G.; Lorenzini, S. FindGeo: A Tool for Determining Metal Coordination Geometry. *Bioinformatics* **2012**, *28*, 1658–1660.
- (70) Garribba, E.; Micera, G. The Determination of the Geometry of Cu(II) Complexes: An EPR Spectroscopy Experiment. *J. Chem. Educ.* **2006**, *83*, 1229.
- (71) Androš, L.; Jurić, M.; Planinić, P.; Žilić, D.; Rakvin, B.; Molčanov, K. New Mononuclear Oxalate Complexes of Copper(II) with 2D and 3D Architectures: Synthesis, Crystal Structures and Spectroscopic Characterization. *Polyhedron* **2010**, *29*, 1291–1298.
- (72) De, A.; Sengupta, A.; Lloret, F.; Mukherjee, R. Chemical Fixation of Atmospheric CO<sub>2</sub> by Copper(II) Complexes of a Tridentate N-Donor Ligand. *Z. Anorg. Allg. Chem.* **2018**, *644*, 801–811.
- (73) Malinina, E. A.; Kochneva, I. K.; Polyakova, I. N.; Avdeeva, V. V.; Buzanov, G. A.; Efimov, N. N.; Ugolkova, E. A.; Minin, V. V.; Kuznetsov, N. T. Structure and Magnetic Properties of Trinuclear Copper(II) Complex [Cu<sub>3</sub>(Bipy)<sub>6</sub>(M<sub>3</sub>-CO<sub>3</sub>)] [B<sub>3</sub>H<sub>3</sub>]<sub>2</sub>·4.5DMF·2H<sub>2</sub>O. *Inorg. Chim. Acta* **2018**, *479*, 249–253.
- (74) Bain, G. A.; Berry, J. F. Diamagnetic Corrections and

- Pascal's Constants. *J. Chem. Educ.* **2008**, *85*, 532.
- (75) CrysAlisPro, Version 1.171.37.35, Rigaku OD, **2014**.
- (76) Burla, M. C.; Caliandro, R.; Camalli, M.; Carrozzini, B.; Cascarano, G. L.; Giacovazzo, C.; Mallamo, M.; Mazzone, A.; Polidori, G.; Spagna, R. SIR2011: A New Package for Crystal Structure Determination and Refinement. *J. Appl. Crystallogr.* **2012**, *45*, 357–361.
- (77) Sheldrick, G. M. A Short History of SHELX. *Acta Crystallogr. A.* **2008**, *64*, 112–122.
- (78) Aroyo, M. I.; Perez-Mato, J. M.; Capillas, C.; Kroumova, E.; Ivantchev, S.; Madariaga, G.; Kirov, A.; Wondratschek, H. Bilbao Crystallographic Server: I. Databases and Crystallographic Computing Programs. *Z. Kristallogr. Cryst. Mater.* **2009**, 15–27.
- (79) Jacques, J.; Collet, A.; Wilen, S. H. *Enantiomers, Racemates, and Resolutions*; Wiley, **1981**.
- (80) Eliel, E. L.; Wilen, S. H.; Doyle, M. P. *Basic Organic Stereochemistry*; Wiley-Interscience: New York, **2001**.
- (81) Allen, J. J.; Barron, A. R. Refinement of Crystallographic Disorder in the Tetrafluoroborate Anion. In *Physical Methods in Chemistry and Nano Science*; Rice University, **2011**.
- (82) Spek, A. Single-Crystal Structure Validation with the Program PLATON. *J. Appl. Crystallogr.* **2003**, *36*, 7–13.
- (83) van der Sluis, P.; Spek, A. L. BYPASS: An Effective Method for the Refinement of Crystal Structures Containing Disordered Solvent Regions. *Acta Cryst.* **1990**, *46*, 194–201.
- (84) Amin, E. A.; Truhlar, D. G. Zn Coordination Chemistry: Development of Benchmark Suites for Geometries, Dipole Moments, and Bond Dissociation Energies and Their Use To Test and Validate Density Functionals and Molecular Orbital Theory. *J. Chem. Theory Comput.* **2008**, *4*, 75–85.
- (85) Cramer, C. J.; Truhlar, D. G. Density Functional Theory for Transition Metals and Transition Metal Chemistry. *Phys. Chem. Chem. Phys.* **2009**, *11*, 10757–10816.
- (86) Gaussian 16, Revision C.01, Frisch, M. J.; Trucks, G. W.; Schlegel, H. B.; Scuseria, G. E.; Robb, M. A.; Cheeseman, J. R.; Scalmani, G.; Barone, V.; Petersson, G. A.; Nakatsuji, H.; Li, X.; Caricato, M.; Marenich, A. V.; Bloino, J.; Janesko, B. G.; Gomperts, R.; Mennucci, B.; Hratchian, H. P.; Ortiz, J. V.; Izmaylov, A. F.; Sonnenberg, J. L.; Williams-Young, D.; Ding, F.; Lipparini, F.; Egidi, F.; Goings, J.; Peng, B.; Petrone, A.; Henderson, T.; Ranasinghe, D.; Zakrzewski, V. G.; Gao, J.; Rega, N.; Zheng, G.; Liang, W.; Hada, M.; Ehara, M.; Toyota, K.; Fukuda, R.; Hasegawa, J.; Ishida, M.; Nakajima, T.; Honda, Y.; Kitao, O.; Nakai, H.; Vreven, T.; Throssell, K.; Montgomery, J. A., Jr.; Peralta, J. E.; Ogliaro, F.; Bearpark, M. J.; Heyd, J. J.; Brothers, E. N.; Kudin, K. N.; Staroverov, V. N.; Keith, T. A.; Kobayashi, R.; Normand, J.; Raghavachari, K.; Rendell, A. P.; Burant, J. C.; Iyengar, S. S.; Tomasi, J.; Cossi, M.; Millam, J. M.; Klene, M.; Adamo, C.; Cammi, R.; Ochterski, J. W.; Martin, R. L.; Morokuma, K.; Farkas, O.; Foresman, J. B.; Fox, D. J. Gaussian, Inc., Wallingford CT, **2016**.

## For Table of Contents Use Only

## Structural Variety of Isopropyl-bis(2-picolyl)amine Complexes with Zinc(II) and Copper(II)

Natalija Pantalon Juraj,<sup>a</sup> Senada Muratović,<sup>a</sup> Berislav Perić,<sup>a</sup> Nataša Šijaković Vujičić,<sup>a</sup> Robert Vianello,<sup>a</sup> Dijana Žilić,<sup>a</sup> Zvonko Jagličić<sup>b</sup> and Srećko I. Kirin<sup>a,\*</sup>



The formation of different Zn(II) and Cu(II) complexes of the *iPr-bpa* ligand was affected by counterions of different coordinating ability, forming monomers, dimers, a cyclic trimer and a coordination polymer.